Pieńkowski *et al.*
Progress in Earth and Planetary Science (2024) 11:18
https://doi.org/10.1186/s40645-024-00612-3

Progress in Earth and Planetary Science

RESEARCH ARTICLE

Open Access

Early Jurassic extrinsic solar system dynamics versus intrinsic Earth processes: Toarcian sedimentation and benthic life in deep-sea contourite drift facies, Cardigan Bay Basin, UK

Grzegorz Pieńkowski[1^], Alfred Uchman[2*], Krzysztof Ninard[2], Kevin N. Page[3] and Stephen P. Hesselbo[3]

Abstract

The Cardigan Bay Basin (UK) may have functioned as a deep and narrow strait, and thereby influenced Early Jurassic oceanic circulation through the northern and southern Laurasian Seaway, and between Boreal and Peri-Tethys domains. Toarcian hemipelagic deposits of the basin in the Mochras borehole show strongly bioturbated contourite facies. Trace fossils are strongly dominated by *Phycosiphon incertum* (represented by four morphotypes), which was produced by opportunistic colonizers. *Thalassinoides*, *Schaubcylindrichnus* and *Trichichnus* are common (the latter is a deep-tier trace fossil produced by filamentous sulfide-oxidizing bacteria with a high tolerance for dysoxia), accompanied by less common *Zoophycos*, *Planolites*, *Palaeophycus*, *Teichichnus*, *Rhizocorallium*, *Chondrites,* and dwelling and resting structures, such as cf. *Polykladichnus*, *Siphonichnus*, *Skolithos*, *Arenicolites*, *Monocraterion* and *Lockeia*. Ichnological and lithological signals suggest repetitive fluctuations in benthic conditions attributed to a hierarchy of orbital cycles (precession and obliquity [4th order], short eccentricity [3rd order], long eccentricity [2nd order] and Earth–Mars secular resonance [1st order]). The Pliensbachian–Toarcian transition appears to be a significant palaeoceanographic turning point in the Cardigan Bay Basin, starting a $CaCO_3$ decline, and with the most severe oxygen crisis of the Tenuicostatum Zone (here dysoxic but not anoxic) ending at the onset, in the early Serpentinum Zone (Exaratum Subzone), of the Toarcian negative carbon isotope excursion (To-CIE—linked with the Toarcian Oceanic Anoxic Event occurring in the lower part in the Serpentinum Zone). This trend contrasts with the prevalence of anoxia synchronous with the To-CIE in many other settings. Minor dysoxia returned to the Mochras setting in the latest Thouarsense to Dispansum zone interval. Extreme climate warming during the To-CIE may have enhanced and caused a reversal in the direction of deep marine circulation, improving oxygenation of the sea floor. Spectral analysis of binary data on ichnotaxa appearances gives high confidence in orbital signals and allows refined estimation of ammonite zones and the duration of the Toarcian (minimum ~ 9.4 Myr).

Keywords Hemipelagic contourites, Deep sea circulation, Climate, Trace fossils, Orbital forcing, Toarcian astrochronology

[^]Grzegorz Pieńkowski: died in April 2023.

*Correspondence:
Alfred Uchman
alfred.uchman@uj.edu.pl
Full list of author information is available at the end of the article

1 Introduction

The impact of orbital forcing versus internal Earth processes on climate change through Earth history is an important topic of debate (e.g., Lourens 2021). Here, the influence of these factors on the Earth system in the deep geological past (the Toarcian age, Early Jurassic epoch), over the course of about 10 Myr, is discussed in relation to major climate changes and deep-sea circulation. The Llanbedr (Mochras Farm) borehole, hereafter referred to as Mochras, is situated in the Cardigan Bay Basin (Wales, UK) and cored an unusually thick (~1300 m) Early Jurassic age succession, with relative completeness of ammonite chronozones (Woodland 1971). During the Early Jurassic, this extensional basin was located at a mid-palaeolatitude (*c.* 35–40°N), on the NW fringe of the European shelf and within the Laurasian Seaway (Fig. 1). The Toarcian part of the core has been studied in many respects, including biostratigraphy (Woodland 1971; Page in Copestake and Johnson 2014; McArthur et al. 2016), lithology (Woodland 1971; Dobson and Whittington 1987; Hesselbo et al. 2013; Copestake and Johnson 2014; McArthur et al. 2016), carbon cycle and climate-driven local sedimentary processes (Jenkyns et al. 2002; Xu et al. 2018a), ostracod and foraminiferal assemblages (Boomer 1991; Copestake and Johnson 2014; Reolid et al. 2019; Rodríguez-Tovar et al. 2020), magnetostratigraphy (Xu et al. 2018b), and calcareous nannofossils and primary productivity (Bown 1987; Menini et al. 2021; Paulsen and Thibault 2023). A chemostratigraphic reference record shows a major ~ 7‰ negative excursion in $\delta^{13}C_{TOC}$, associated with the Toarcian Oceanic Anoxic Event (T-OAE) preceded and followed by early Toarcian positive excursions (Jenkyns et al. 2002; Xu et al. 2018b). Climate-driven, accelerated continental weathering and hydrological cycling was suggested as the cause of intensified sediment supply to the Cardigan Bay Basin (Xu et al. 2018a, b). However, a more focussed characterization of sedimentary environment, ichnology, and benthic life conditions has not yet been published.

The prominent expression of Carbon Isotope Excursions (CIEs) in Mochras with an amplitude of about one per mil in $\delta^{13}C_{TOC}$ (Xu et al. 2018a) testifies to the expanded and relatively complete stratigraphic record therein, particularly in the early Hettangian and Sinemurian age part of the section, allowing for a distinction between intrinsic Earth processes and extrinsic solar system dynamics as the driving mechanisms for the Early Jurassic $\delta^{13}C$ fluctuations (Xu et al. 2018a; Storm et al. 2020; Hollaar et al. 2023; Hesselbo et al. 2023).

The duration of the whole Toarcian, based on astronomical calibration is not well constrained to date. Time series of magnetic susceptibility (Huret et al. 2008) and XRF-derived Ti content from the Sancerre borehole, Paris Basin, France, has been used, which yielded a minimum duration of 8.3 Myr from 405-kyr long eccentricity cycles (Boulila et al. 2014, 2019), a result largely confirmed by Huang (2018). Nonetheless, numerous studies of the T-OAE CIE interval itself have not yet resulted in a consensus on duration, with estimates varying widely. It has been estimated to be ~ 300 to ~ 500 kyr (Kemp et al. 2005, 2011; Boulila et al. 2014, 2019; Boulila and Hinnov 2017; Ikeda et al. 2018) or ~ 900 kyr (Suan et al. 2008; Huang and Hesselbo 2014).

In this paper, detailed sedimentological and ichnological data are presented. They allow recognition of ecological parameters, as trace fossils are sensitive in situ indicators of even very subtle environmental changes such as current strengths, oxygen content, food supply, and stability of the environment, allowing for new interpretations and correction of existing ones, based on other proxies. Furthermore, deep-sea environmental changes using both new and existing data ($\delta^{13}C_{TOC}$, calcium content, organic geochemistry, benthic fossils—Xu et al. 2018a; Reolid et al. 2019) are discussed to determine which changes are caused by intrinsic Earth processes and which can be attributed to extrinsic solar system dynamics, also based on spectral analyses of trace fossil appearances. Benthic invertebrates respond to various environmental changes driven by orbital forcing (e.g., Wetzel 1991; Erba and Premoli Silva 1994; Hüneke and Stow 2008; Pervesler et al. 2008; Rebesco et al. 2014), although the mechanisms of control are still poorly understood. In the present study we document and analyse lithological and ichnological cycles that can be related to orbital controls, and by this means provide a new estimate of the duration of the Toarcian and ammonite zones within this stage.

2 Material and methods

The Mochras slabbed core (in 1 m core sections) is held at the British Geological Survey, Keyworth, Nottingham, UK. A nearly continuous 261 m-thick section of core was investigated using standard visual sedimentological description at centimetre scale accuracy (Fig. 2a, b) with special attention paid to the integration of sedimentological and ichnological observations. Depths in Figs. 2a, b and 3 are referred to metres below surface (mbs). Alternative descriptive classifications were adopted—for siliciclastic sections, the classical array of claystone-mudstone-siltstone-sandstone-conglomerate was used, while in sections with high carbonate content (over 30–40%) the classification of carbonate rock lithotypes based on Dunham (1962) was used (mudstone-wackestone-packstone-grainstone; Figs. 2a, b and 4, 5, 6). Based on ammonite occurrences intervals have been assigned to chronozones as documented most recently in McArthur

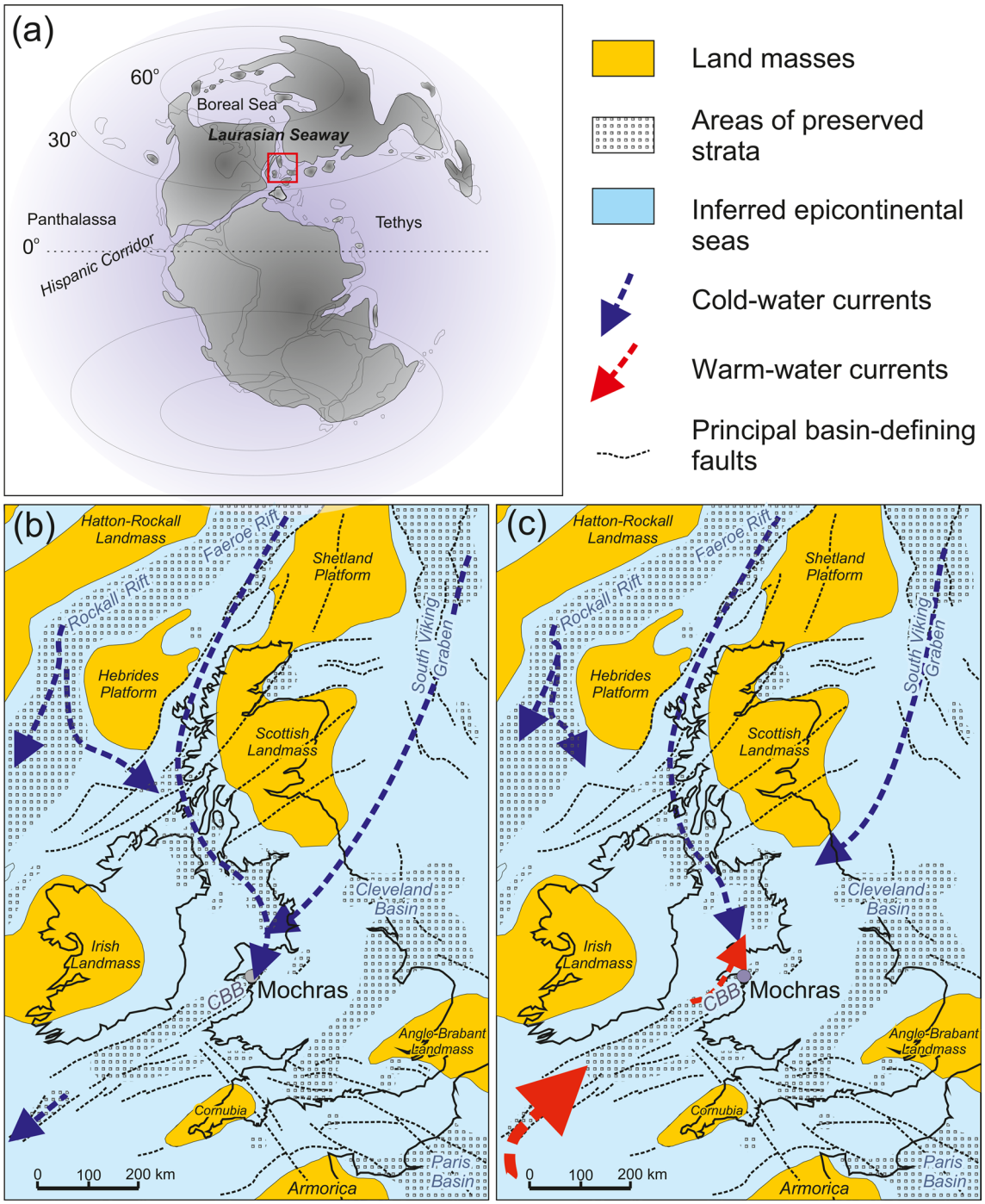

Fig. 1 Location maps. **a** Toarcian palaeogeography with localization of the Laurasian Seaway and Mochras borehole. **b** Enlargement of the area in the frame **a** showing major basins and elevated areas in the Toarcian times (after Cope et al. 1992, amended) and enhanced thermohaline circulation from the North from the late Falciferum Subzone on, with generally improved oxygenation of the bottom (circulation intensity and average oxygenation achieved its highest level in the late Bifrons and Variabilis to earliest Thouarsense zones. *CBB* Cardigan Bay Basin. **c** The same map showing the inferred current flow paths during the Tenuicostatum Zone–Exaratum Subzone and), the latest Thouarsense–Dispansum Zone and (to a lesser extent) Pseudoradiosa Zone thermal anomalies related to a strengthening of warm equatorial Tethyan westward currents and associated with the conspicuous ichnodiversity/oxygenation crisis in Mochras. Note the pivotal position of the Cardigan Bay Strait (now Cardigan Bay Basin – CBB) in the Laurasian Seaway between Boreal Sea and Peri-Tethys domain

et al. (2016); here we follow convention and use roman type to denote chonozones (see discussion of distinction between biozones and chronozones in Jurassic stratigraphy in Hesselbo et al. 2020a).

For numerical cyclicity (spectral) analysis, occurrences of trace fossils *Phycosiphon* morphotypes 2, 3, *Thalassinoides, Schaubcylindrichnus, Planolites* and *Trichichnus* (Figs. 2a, b, 5, 7 and 8), as well as intervals with preserved lamination and undulated bedding (see below) were used to compile discrete binary time series. Ranges of trace fossils, undulated bedding and lamination were digitized by visual sampling with an even step of 10 cm. Resultant time series consist of approximately 2550 binary digits each (Additional file 1).

To allow comparison between the ichnological record and existing $\delta^{13}C_{TOC}$, TOC content, Ca content, Zr/Rb, Ti/Al, Si/Al and gamma ray records, curves based on smoothed data are juxtaposed (Fig. 3). Ichnological records were converted to curves by applying a smoothing spline algorithm (De Boor 2001) directly to binary time series with smoothing factor values in the 8–9 range, in each case experimentally adjusted to obtain an optimal degree of smoothing.

Geochemical data taken from Xu et al. (2018a, supplementary data sheet) and gamma ray data from Woodland (1971) were subjected to analogous smoothing, with smoothing factor values in the 4–6 range.

The runs test was conducted to confirm statistically that the trace fossils, undulated bedding and lamination occur in a non-random order. This non-parametric test evaluates the null hypothesis of the two states being distributed randomly in a binary time series (Hammer and Harper 2006). For the present study, the adopted hypotheses are:

H_0: distribution of occurrences is random;

H_1: distribution of occurrences is non-random.

Runs are defined as uninterrupted sequences of one state, in the present case either an occurrence (N_1) or non-occurrence (N_2). The null hypothesis can be rejected if the observed number of runs (R) and the number of runs expected for the random time series ($\bar{R}$) are statistically different. PAST 4.0 software (Hammer et al. 2001) was used to compute the test statistic (Z-score). The null hypothesis was rejected at a significance level of 5% if an absolute value of computed Z-score was greater than the critical value of 1.96 taken from a standard normal table (Additional file 2).

A time series, both binary and continuous, can be seen as a sum of component constant-frequency waves. Mathematical transform operations serve as tools to extract the frequencies of component waves from time series. A range of well-established numerical methods that derive from the Fourier transform are applied in the spectral analysis of continuous time series. However, they are not suited for analysis of binary time series (Weedon 2003). Instead, the Walsh transform provides a way to conduct power-spectral analysis of binary data. The Walsh transform outputs the decomposed signal as a function of sequency, which is half of the average number of zero-crossings per unit of space (or time). From the point of view of results interpretation, the Walsh sequency can be equated with commonly recognized concept of frequency. Conceptual basis of the Walsh method and its applicability in cyclostratigraphy have been described by Negi and Tiwari (1984), Weedon (1989), van Echelpoel (1994) and Maiti and Tiwari (2012). According to Tiwari (1987) and Negi et al. (1993) the Walsh analysis not only outputs the peaks related to main orbital periodicities, but their component periodicities and beat periodicities as well.

Binary time series were subjected to analysis using the Walsh transform module implemented in PAST 4.0 software (Hammer et al. 2001). To find the optimal balance between the signal-to-noise ratio and spectral resolution, terminations of binary data series were adjusted by trial and error. Obtained power-spectra display peaks in the stratigraphic thickness domain (number of cycles per one metre, Fig. 9). Conversion of peak values from the thickness domain into the time domain was based on two alternative assumed average sedimentation rate value of 4.6 cm/kyr (upper number in the Fig. 9) and

(See figure on next page.)

Fig. 2 Investigated part of the Mochras Borehole showing stratigraphy (stages, ammonite zones, and subzones), lithology, ichnology and geochemistry of the Toarcian section. **a** Tenuicostatum and Serpentinum zones. **b** Bifrons–Aalensis zones. O, other, rarely occurring trace fossils: *Ar*, *Arenicolites*; *Ast*, *Asterosoma*; *Ch*, *Chondrites*; *Lo*, *Lockeia*; *Mon*, *Monocraterion*; *Pol*, cf. *Polykladichnus*; *Rh*, *Rhizocorallium*; *Sip*, *Siphonichnus*; *Sk*, *Skolithos*. *Trichichnus* (filamentous mat-forming, sulfide-oxidizing bacteria and "pyritized tubes") represent traces of unidentified life activity/disputable origin. Ub—micrite/mudstone of 'massive' appearance, with undulated or cuboid parting. Geochemistry: $\delta^{13}C_{TOC}$—carbon isotope curve (after Xu et al. 2018a); XRF-derived calcium record (after Xu et al. 2018a). Cyclicity: thin dashed lines—4th order (c. 20 kyr) cycles; solid gray lines—3rd order (c. 100 kyr) cycles; red lines—2nd order (c. 405 kyr) cycles; grey bar on the right—1st order (c. 2.5 Myr) cycles expressed in bottom oxygenation (shaded) and ichnology. Foraminiferal biotic crisis after Reolid et al. (2019). Red bars in the metric depth column—position of the sections presented in Fig. 4. Biostratigraphy from Page in Copestake and Johnson (2014) and McArthur et al. (2016) as summarised in Additional file 3

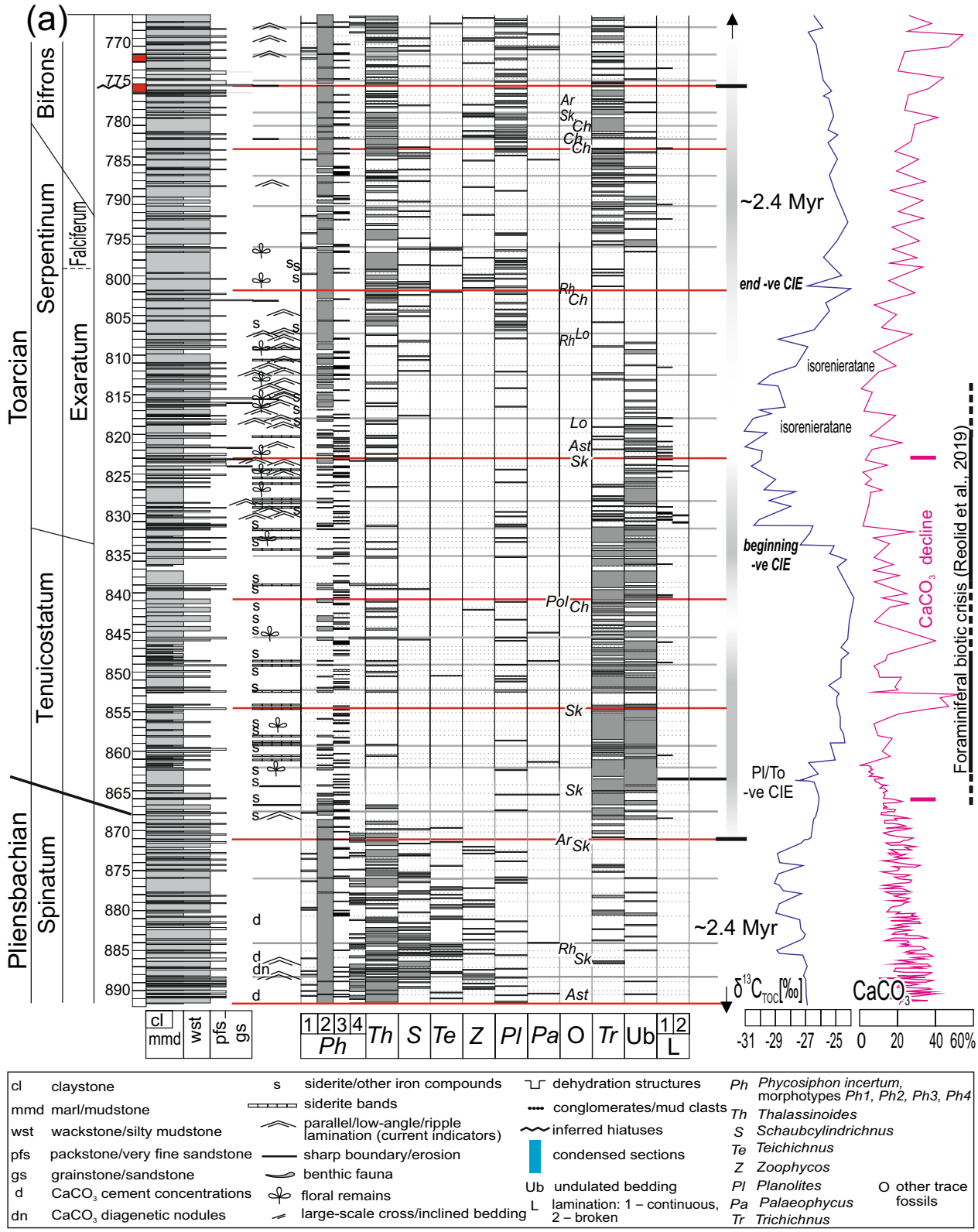

Fig. 2 (See legend on previous page.)

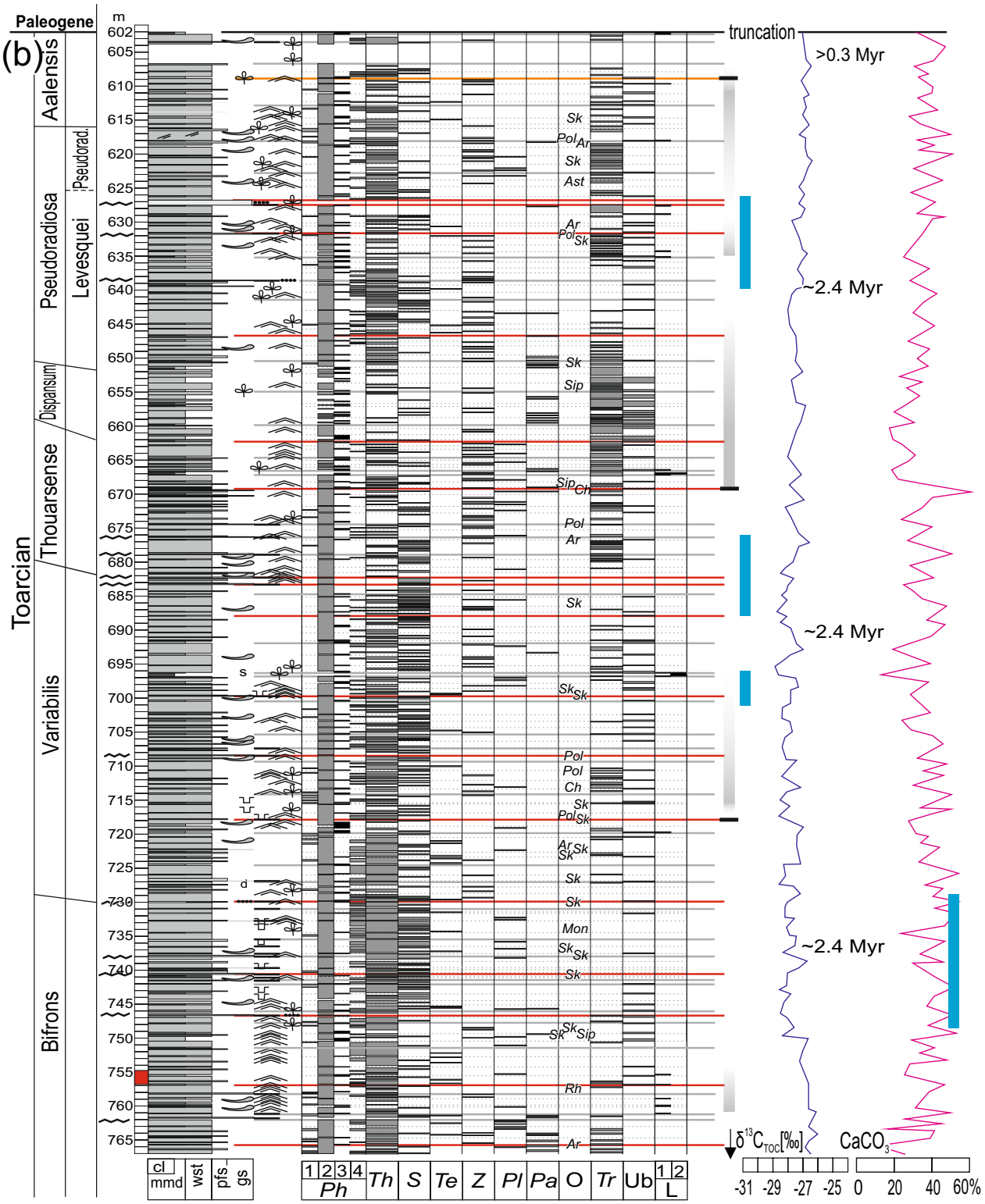

Fig. 2 continued

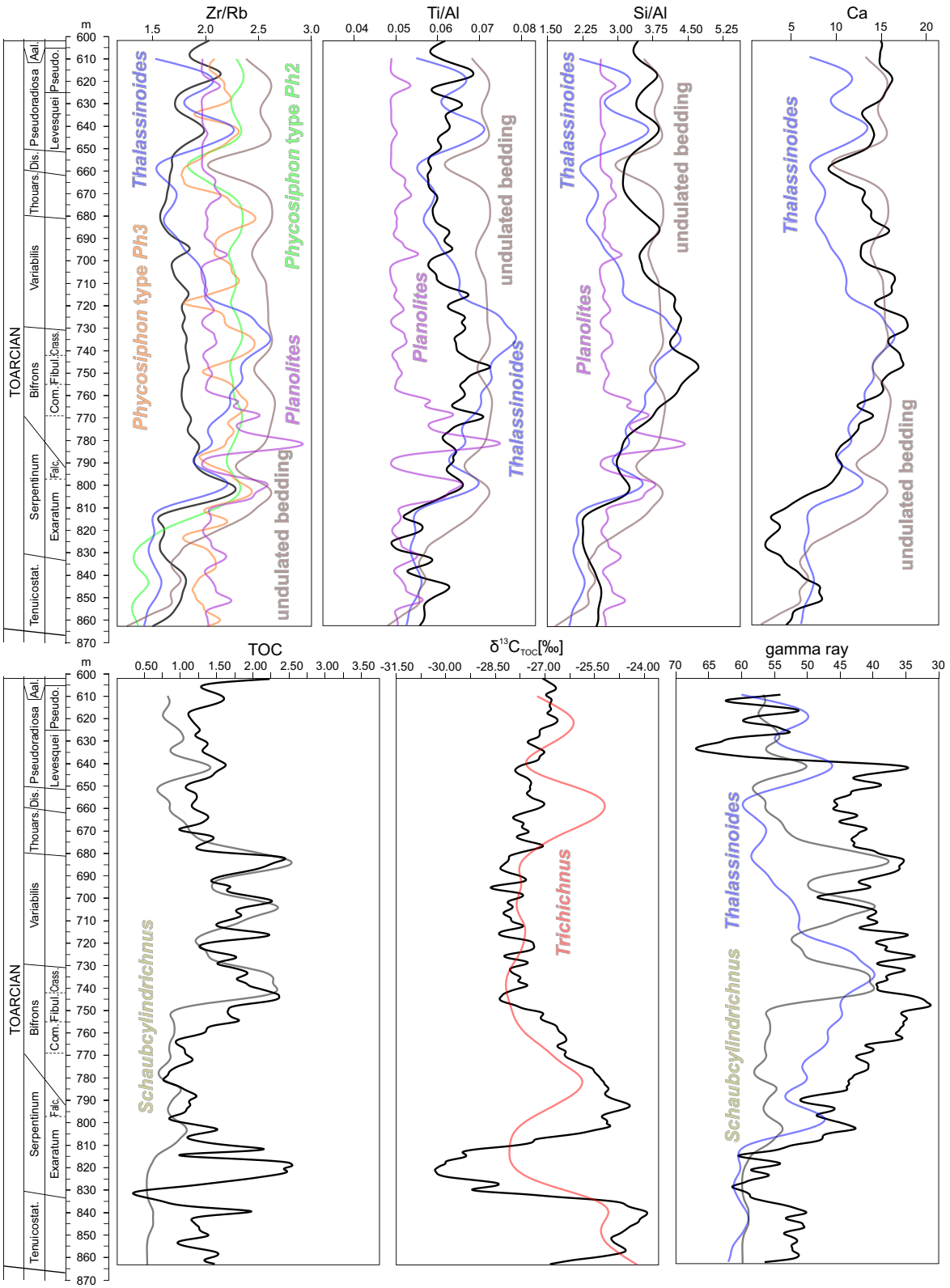

Fig. 3 Smoothing spline-smoothed curves reflecting selected ichnotaxa abundance against the background of geochemical and gamma ray records from the Mochras borehole. Contains British Geological Survey materials © UKRI 2024

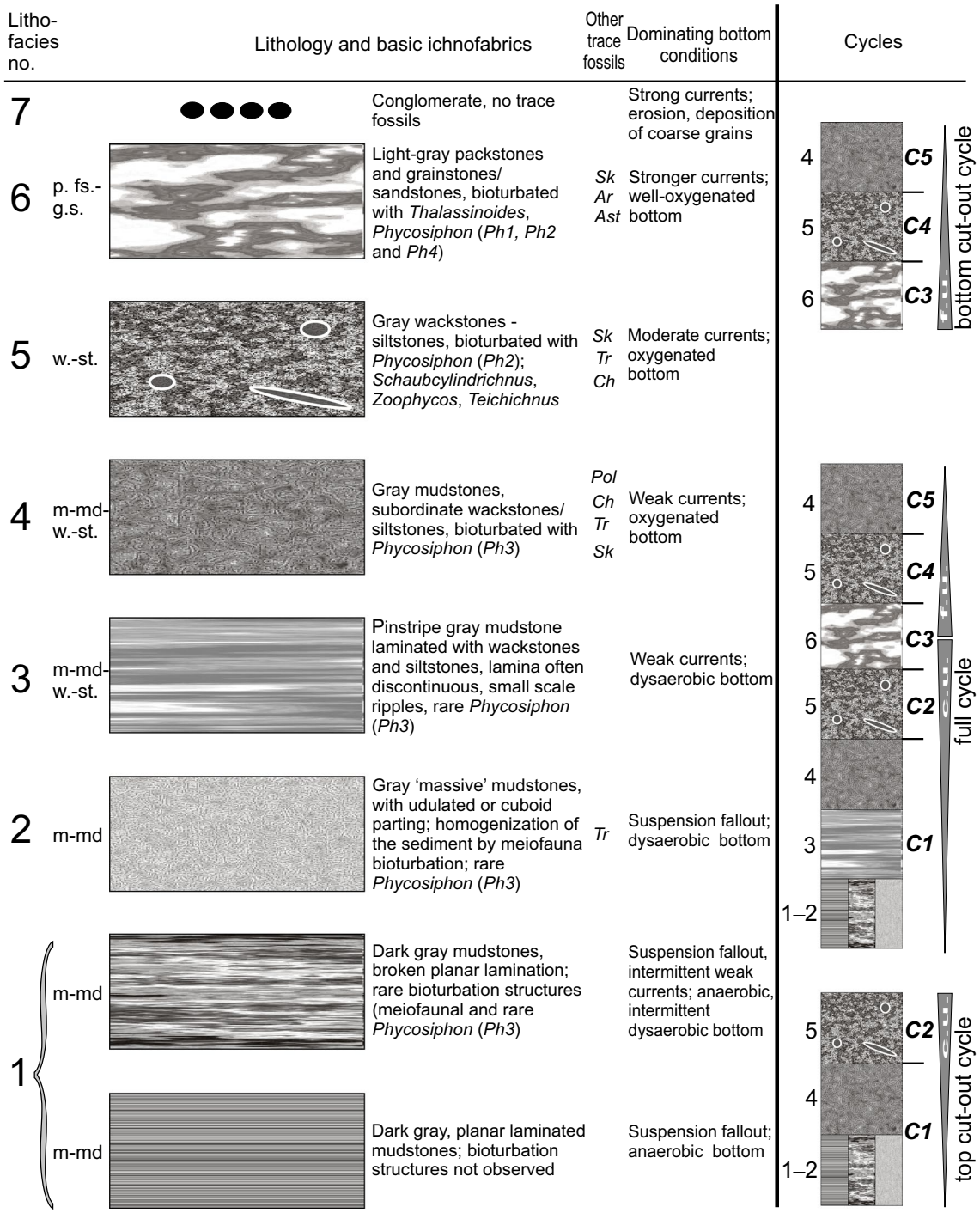

Fig. 4 Seven main lithofacies (1–7) and ichnofabrics in the Mochras profile; to the right—main types of bigradational contourite drift sedimentary cycles built of main lithofacies—full cycle, top cut-out cycle, bottom cut-out cycle (referred to Stow et al. 2002; Stow and Faugeres 2008). Contourite cycle divisions reflect variations in current velocity. C1–C5—"Full" contourite cycle. For lithology and trace fossil abbreviation see Fig. 2a, b

4.1 cm/kyr (lower number in the Fig. 9). Consequently, time values corresponding to peak values were calculated as a proportion of 21,700 and 24,400 yr per one metre, respectively.

The most reliable sedimentation rates can be obtained for the Tenuicostatum Zone (~ Polymorphum Zone), where existing radioisotopic (Sell et al. 2014) and astrochronological (Huang and Hesselbo 2014; Rocha et al.

Fig. 5 Sections of the Mochras core showing common types of lithology, ichnology, and cyclicity of sedimentation. **a** 775.79–776.81 m—bigradational (symmetrical) cycle, with gradually coarsening upward (cu) and gradually fining-upward (fu) phases, cut from the top by a conspicuous erosional surface (red bar), capped by sandstone and fining-upward succession. **b** 772.03–772.97 m—full bigradational (symmetrical) cycle, with gradually coarsening upward (cu) and gradually fining-upward (fu) phases. A and B—no primary sedimentary structures are visible, due to pervasive bioturbation. **c, d** 754.86–756.82 m—bigradational, top-cut cycle, some current ripples can be seen in the middle part; the cycle is followed by mudstone, in places with lamination, passing into the coarsening-upward phase of the next cycle. Characteristic bigradational ("symmetrical") cycles with bioturbated coarser parts result from variations in current velocity and are referred to as contourite cycles (Stow et al. 2002; Stow and Faugeres 2008—see also Fig. 4)

2016; Huang 2018) constraints give duration of ~ 0.8 Myr (although, assuming inferred hiatuses, this duration could be extended to ~ 1 Myr—Ruebsam and Al-Husseini 2020). With 33.8 m of sediments representing this time in Mochras, an average sedimentation rate of 4.1 cm/kyr is calculated. On the other hand, the sedimentation rate in the Pliensbachian section in Mochras (representing a similar depositional setting and stable sedimentation

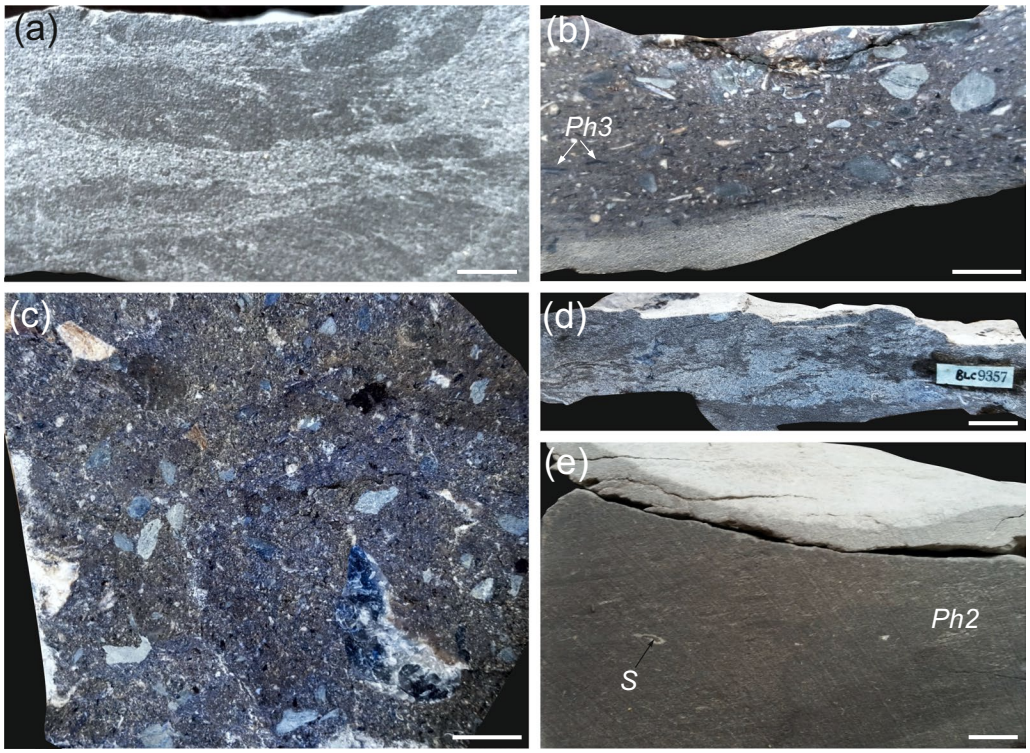

Fig. 6 Some sedimentary features of the investigated section. **a** Rip-up clasts pointing to the high energy of currents and erosion, 746.7 m. **b** Conglomerate resting on an erosional surface. Most pebbles are composed of local material (in some *Phycosiphon incertum* morphotype 3, *Ph3,* is visible), usually cemented by calcium carbonate. Shell debris is also common, 627.4 m. **c** Conglomerate—pebbles are composed of both local and exotic material (e.g., a larger chert pebble in the bottom-left), 627.3 m. **d** Erosional surface with coarse sandstone/grainstone, 630.9 m. **e** Mudstone–wackestone with erosional (channelized) surface and cross-bedded sandstone above. *S*, *Schaubcylindrichnus*; *Ph2*, *Phycosiphon incertum* morphotype 2, 683.3 m

rate) was estimated at about 4.6 cm/kyr (Ruhl et al. 2016; Pieńkowski et al. 2021). Therefore, alternative time values were calculated for peaks in the spectra assuming this value. For comparison, the conversion was also tested with 3.3 and 2.8 cm/kyr sedimentation rates, which could be representative for more condensed sections with less stable sedimentation or more frequent erosional surfaces. However, the results based on these two lower alternative sedimentation rates were discarded as less meaningful.

3 Results

3.1 Lithology and sedimentary structures

The succession primarily comprises siliciclastic and calcareous deposits: mudstone/micrite, siltstone/wackestone and sandstone/grainstone with varying proportions of calcareous and siliceous grains of silt to fine-sand size. The siliciclastic input in coarser silty-sandy lithofacies is more pronounced in the lower part of the section with a $CaCO_3$ content typically between 10 and 30%, while the mudstone contains a greater siliciclastic component and locally (805–840 mbs) is carbonate-free (Fig. 2a; Xu et al. 2018a). Macrofossils are mainly represented by pelagic cephalopods (Xu et al. 2018a; Ullmann et al. 2021). Crinoids are much less common in the Toarcian than in the Pliensbachian section (Pieńkowski et al. 2021) and are most likely redeposited from shallower settings due to their buoyancy (Savarese et al. 1997). Benthic shelly organisms are rare, and they are represented by in situ burrowing bivalves found in a few horizons (Fig. 7c, d). Benthic foraminifers are also present, and their assemblages are important to determine bottom life conditions (Copestake and Johnson 2014; Reolid et al. 2019). Drifted flora occurs locally, mostly in the Tenuicostatum Zone and the Exaratum Subzone, with some occurrences also in the Variabilis Zone. Low-angle cross-lamination is common, particularly in the Exaratum, mid-Bifrons, mid-Variabilis, Thouarsense, and mid-Pseudoradiosa zones. Siderite (usually dispersed, in places forming bands and nodules, oxidised to iron oxide) is common in the Tenuicostatum Zone and Exaratum Subzone, as noted by Xu et al. (2018a). Dewatering/compactional cracks are observed only in a few horizons (in the Bifrons and Variabilis zones).

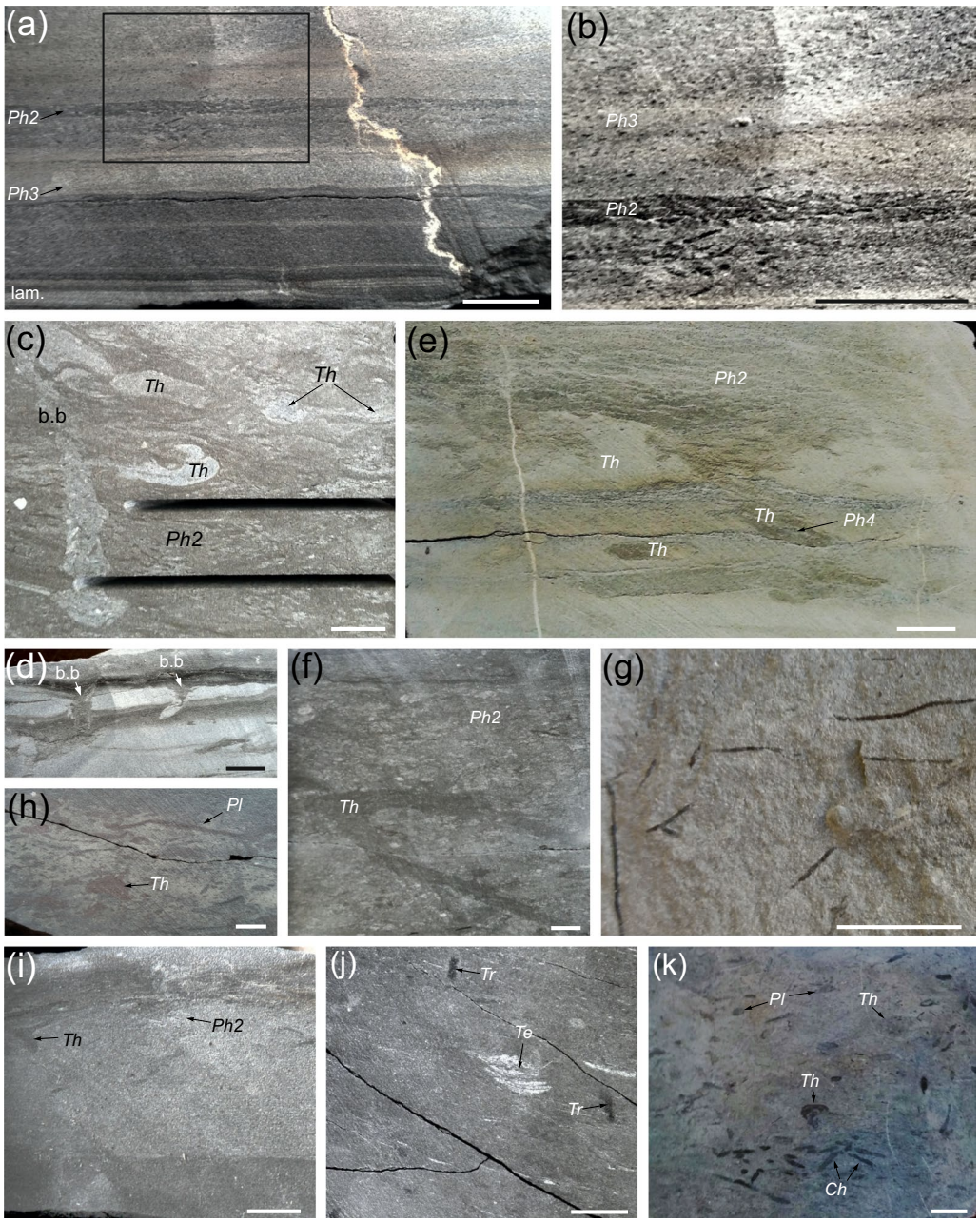

Fig. 7 Sedimentological and ichnological features. **a** Fluctuations of bottom currents: lamination (lam.) in the bottom (stagnation, no trace fossils), followed by altered periods of more stagnant/more dynamic (arrowed) current conditions. Changing oxygenation and nutrient delivery is reflected in different morphotypes of *Phycosiphon incertum* (*Ph2, Ph3*): small *Ph3* (more stagnant conditions) and larger *Ph2* (more dynamic conditions), depth 824.0 m. **b** Enlarged framed fragment of A. **c** Ichnofabric showing succession (tiering) of the earliest/shallowest *Phycosiphon incertum* morphotype 2 (*Ph2*), followed by *Thalassinoides* (*Th*) and bivalve burrow (b.b.), 603.6 m. **d** Cross-bedded (low-angle), very fine sandstone with mudstone intercalations. Bivalve resting trace ?*Lockeia* (b.b.), 818.67 m. **e** *Thalassinoides* burrow systems (*Th*) in siltstone/sandstone, in places infilled by *Phycosiphon incertum* morphotype 4 (*Ph4*)—arrowed. Numerous *Phycosiphon incertum* morphotype 2 (*Ph2*) in the background, 823.35 m. **f** *Thalassinoides* galleries of tubular burrows (*Th*, deeper tier), *Phycosiphon incertum* morphotype 2 (*Ph2*, shallower tier) in the background, 726.1 m. (**g**) *Trichichnus*—pyritized horizontal and oblique, unbranched or branched, thread-like, cylindrical structure produced by bacteria consortium, 712.6 m. **h** *Planolites* (*Pl*—thinner, randomly oriented tubes) and *Thalassinoides* (*Th*—larger burrows), 782.7 m. **i** Post-depositional colonization of a sandstone/grainstone bed with *Phycosiphon incertum* morphotype 2 (*Ph2*, earlier stage—shallower tier) and *Thalassinoides* isp. (*Th*, later stage—deeper tier), 821.6 m. **j** *Teichichnus* (*Te*, shallow tier) and pyritized, aggregated *Trichichnus* cylindrical vertical structures (*Tr*, deeper tier), 850.5 m. **k** *Chondrites* (*Ch*, deep tier) and shallow tier *Thalassinoides* (*Th*) and *Planolites* (*Pl*), 669.5 m. Scale = 1 cm

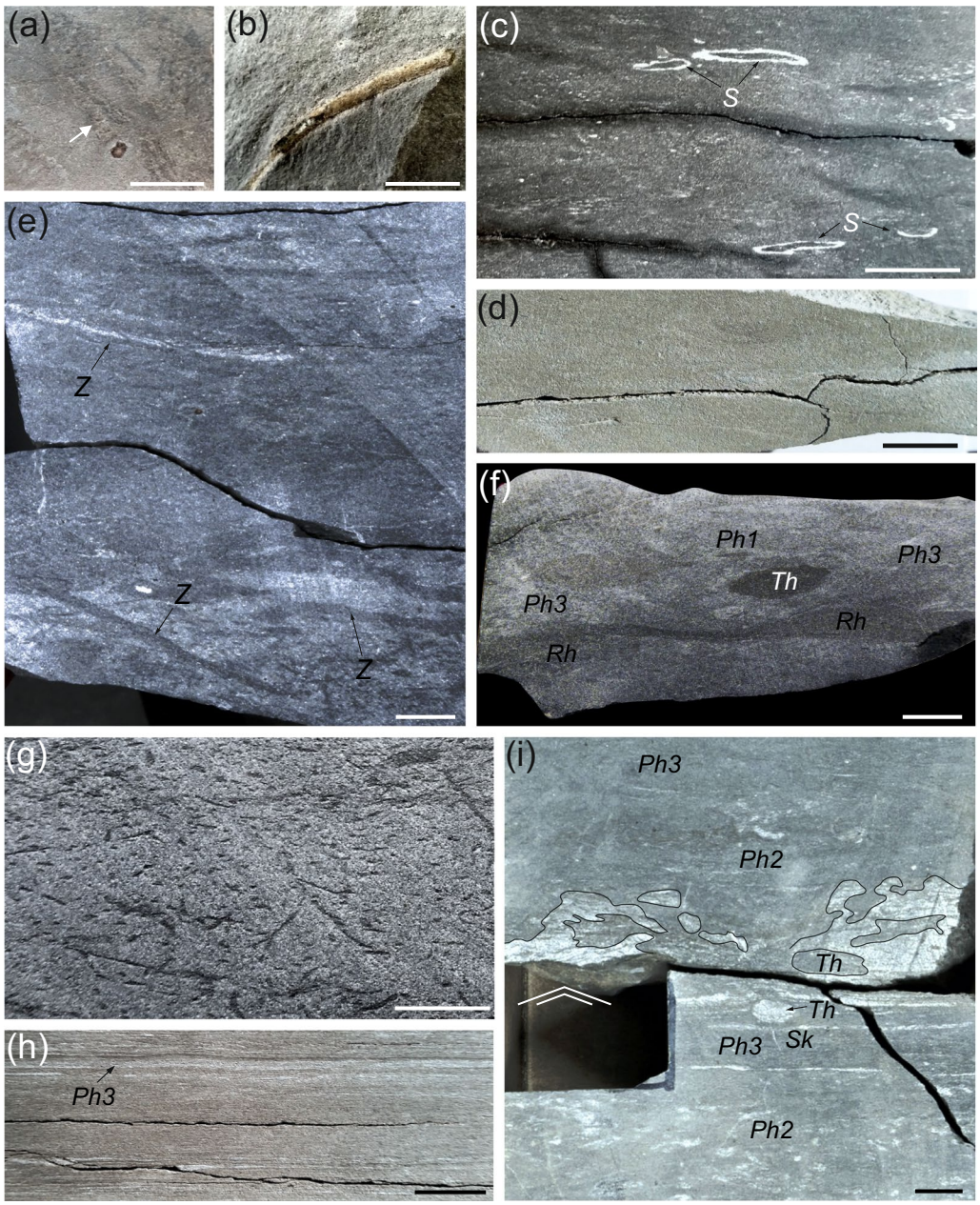

Fig. 8 Other ichnological features. **a** *Phycosiphon incertum* morphotype 2—spreiten burrows visible in horizontal section. This level contains isorenieratane (Xu et al. 2018a, b); in that case, this biomarker does not indicate anoxic bottom conditions, 811.60 m. **b** *Palaeophycus*—cylindrical, pyritized structure with conspicuous lining, 785.2 m. **c** *Schaubcylindrichnus* (*S*)—cylindrical, lined structures flattened by compaction, 702.5 m. **d** Mottled mudstone ("undulated bedding"), sediment homogenized by meiofauna activity. This level contains isorenieratane (Xu et al. 2018a, b); in that case, this biomarker does not indicate permanent anoxic bottom conditions, 819.2 m. **e** *Zoophycos* galleries (*Z*) composed of fan-like, spreiten structures, 782.6 m. **f** *Rhizocorallium* (*Rh*), *Thalassinoides* (*Th*) and *Phycosiphon incertum* morphotypes 1 (*Ph1*) and 3 (*Ph3*), 801.8 m. **g** *Chondrites,* 803.1 m. **h** Lamination in claystone/mudstone, in places broken by bioturbation (*Phycosiphon incertum* morphotype 2, *Ph2*). In the lower and upper part "pinstripe" broken lamination with silty lamina and incipient ripples indicate recurrent activity of weak currents. Despite the presence of isorenieratane in this interval (Xu et al. 2018a, b), current activity and the presence of bioturbation do not support for anoxic conditions on the bottom surface. Depth 811.60 m. **i** Stiff ground and uneven omission surface with *Thalassinoides* (*Th*) and *Skolithos* (*Sk*); *Phycosiphon incertum* morphotypes 2 (*Ph2*) and 3 (*Ph3*) were left in soft sediment. Depth 730.0 m. Scale = 1 cm

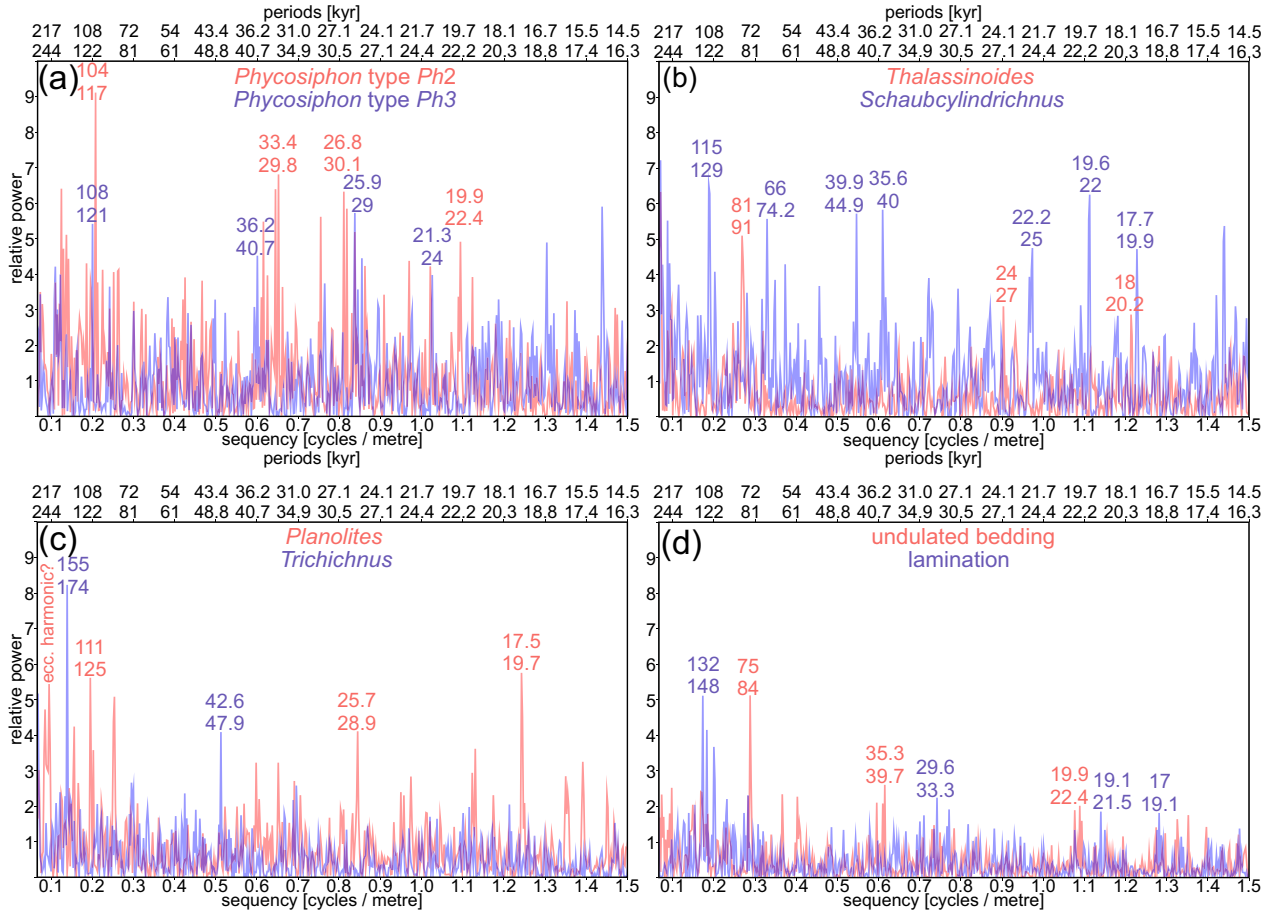

Fig. 9 Overlapping Walsh power-spectra of the time series based on: **a** *Phycosiphon* morphotypes *Ph2* and *Ph3*. **b** *Thalassinoides* and *Schaubcylindrichnus*. **c** *Planolites* and *Trichichnus*. **d** Undulated bedding and lamination. Spectra are scaled true to analysis results (not rescaled). Calculated time values assigned to peaks and upper abscissa axes based on two alternative sedimentation rates 4.6 cm/kyr (upper number) and 4.1 cm/kyr (lower number)

As in the Pliensbachian section, the same six main lithofacies types (Pieńkowski et al. 2021; their Fig. 8) are identified in the Toarcian section of Mochras: (1) Dark grey, planar-laminated siliceous or calcareous micritic mudstone and siliceous claystone with continuous (without bioturbation) and broken lamination (with few bioturbation structures); (2) Massive, poorly bedded mudstone/carbonaceous micritic mudstone, in some cases showing centimetre- to decimetre-scale banding with faint, slightly undulated (undulated bedding), or cuboid parting, which is connected to homogenization by meiofaunal bioturbation of sub-millimetre size (Figs. 4, 5 and 8d); discrete trace fossils are relatively rare; (3) Pinstripe carbonaceous mudstone that is laminated with wackestone-siltstone, in which planar laminae are often discontinuous and lenticular to wavy, planar parallel, or low angle cross-lamination, starved ripples are present, and bioturbation structures can obliterate these in mottled mudstone-wackestone (Figs. 4 and 5); (4) Interlaminated, heterolithic siltstone or wackestone with mudstone, usually bioturbated, with only local sedimentary structures; this lithofacies shows irregular arrangement of mudstone, wackestone-siltstone or grainstone-sandy siltstone in pockets, lenses and streaks, and less commonly, a rapid alternation of thin irregular layers of these three lithologies (Figs. 4 and 5); (5) Packstone/siltstone to very fine sandstone, with primary sedimentary structures—usually obliterated by bioturbation—including parallel bedding and small-scale cross-bedding (Figs. 4 and 5); (6) Sandstone-grainstone, usually bioturbated, with primary structures (parallel bedding and cross-bedding) observed in some horizons (Fig. 4). Additionally, the conglomerate lithofacies (7) is present—it is too rare to play an important role in basic models of cycles, but the presence of conglomerate beds (composed both of local and exotic material—Fig. 6a–c) is important as an indicator of intermittent high-energy currents. Also of

note (compared to Pliensbachian) is a general rarity of lamination.

Contacts between these different lithofacies may be either gradational, yielding indistinct bedding (Figs. 4 and 5), or sharper due to the erosive action of relatively strong bottom currents, thereby yielding more distinct bedding (Figs. 4–6). Compared to the Pliensbachian section (Pieńkowski et al. 2021) of note are much more common sharp, erosional boundaries in the Mochras Toarcian section, associated with coarse-grained sediments (including conglomerates, either with clay pebbles derived from local compacted mudstone or of exotic lithology such as limestone and chert), pointing to high-velocity currents, erosion/non-sedimentation and hiatuses (Fig. 6). In places, hiatal levels are marked by induration of the sediment surface occurring as semi-consolidated/firm muddy/silty substrates with sharp-walled, unlined, uncompacted passively filled burrows (Fig. 7i).

Lithofacies types 1–7 and related ichnofabric in the Toarcian of Mochras are not arranged randomly, but appear in a cyclical order (Figs. 2a, b, 4 and 5). Fully developed, usually 0.5–3 m thick, bigradational grading sequences (some 'couplets' of previous authors) commonly begin from mudstone lithofacies type 2 (representing mixed layer, mottled by burrowing activity of the meiofauna), or mudstone lithofacies type 1 (laminated), gradually passing into lithofacies type 3—pinstripe mudstones with ripple-drift cross laminated siltstones, or lithofacies 4—bioturbated mudstone-wackestone, followed usually by bioturbated wackestone-siltstone and packstone-grainstone with traces of stronger currents (Fig. 5). Above this coarsening-upward part is a fining-upward suite, developed in reverse order, although less complete; usually only lithofacies types 6–5–4 are present. This fining-upward phase of the sequence is usually thinner than the coarsening-upward phase. In some cases, the whole sequence is incomplete; either top or bottom parts can be missing (top cut-out cycles or bottom cut-out cycles—Fig. 5). These successions are like those observed in the Pliensbachian part of the section (Pieńkowski et al. 2021). The main difference is the more common occurrences of erosion surfaces in the Toarcian section, locally with lithofacies type 7 and hiatuses (Fig. 6). Of note are also the markedly finer sediments occurring of earliest Toarcian age (Tenuicostatum Zone, and ealiest Exaratum Subzone) and again in the Thouarsense-Dispansum zonal transition (Figs. 2, 3).

3.2 Trace fossils, ichnofabrics

Trace fossils exhibit sharp outlines and possess a characteristic geometry that allows their classification in terms of ichnotaxonomy, while bioturbation structures have less distinct outlines and do not display a recurrent geometry (Wetzel and Uchman 2012). Below, trace fossils are briefly described. The trace fossils show significant similarities to those described in Pieńkowski et al. (2021) from the Pliensbachian. Their synopsis is presented in Table 1.

Phycosiphon incertum with its four morphotypes (*Ph1, Ph2, Ph3, Ph4*) is the most abundant trace fossil in the Mochras Toarcian. The exception is the Tenuicostatum Zone (and to a lesser extent also the Thouarsense-Dispansum zonal transition), characterised by *Phycosiphon* scarcity and dominance of *Trichichnus*. Previous ichnological analysis of contourites has revealed changes in ichnofabric attributes over relatively short lateral distances, including trace fossil composition, cross-cutting relationships, or ichnofabric index (Hüneke and Stow 2008; Wetzel et al. 2008; Wetzel and Uchman 2012; Rodríguez-Tovar et al. 2016, 2017; Rodriguez-Tovar and Molina 2018). Recently, Dorador et al. (2019) and Pieńkowski et al. (2021) have indicated that the distance to the bottom current 'core' exerts a tangible and widespread influence on specific macro-benthic tracemaker communities in contourite deposits. This parameter itself reflects other bottom current features, such as hydrodynamic energy, grain size, nutrient transport, etc. Specifically, strong domination of *Phycosiphon* is unique for the Pliensbachian-Toarcian contourite deposits in Mochras. *Phycosiphon*, common in turbidites and hyperpycnites (e.g., Wetzel and Uchman 2012; Knaust et al. 2014), is also reported from contourite deposits (Baldwin and McCave 1999; Wetzel et al. 2008) but as a rare, subordinate trace fossil. Lack of *Phycosiphon* in other contourite deposits may be more apparent than real: in previous papers diffuse *Phycosiphon* burrows may simply have been described as "bioturbation". In particular, this ichnotaxon could be difficult to recognize in recent unconsolidated contourite deposits. Other deposit-feeding feeding traces, e.g., *Rhizocorallium*, are rare.

Schaubcylindrichnus isp. is common through the late Bifrons and Variabilis zone strata. In the Toarcian of Mochras, *Teichichnus* isp. is much less numerous than in the Pliensbachian (Pieńkowski et al. 2021). *Teichichnus* and *Schaubcylindrichnus* do not usually occur together. *Thalassinoides* crosscuts *Phycosiphon* of the morphotypes *Ph1, Ph2* and *Ph3*, but is cut by *Ph4*, *Schaubcylindrichnus* and *Teichichnus*. *Trichichnus* (relatively rare in Pliensbachian in Mochras, see Pieńkowski et al. 2021) is particularly common in the Tenuicostatum Zone, which is associated with declining abundance in *Phycosiphon* and low ichnodiversity. *Trichichnus* is also abundant in the mid-Falciferum Subzone, in the Thouarsense-Dispansum zone transition, and (less abundantly) in the mid-Pseudoradiosa Zone. The presence of *Trichichnus* usually points to oxygen-depleted conditions, but interpretation

Table 1 Trace fossils of the Toarcian deposits in the Mochras core

Ichnotaxon	Description	Interpretations and the basic references
Arenicolites isp.	U-shaped, tilted tube, 1.5–4 mm in dimeter. The width is increasing towards the top of the limbs. The trace fossil is 22 mm wide and up to 13 mm deep	A dwelling and feeding burrow of suspension-feeding annelids (e.g., Hakes 1976) or small crustaceans (Goldring 1962). It occurs mostly shallow-marine settings (Crimes 1977), especially in storm beds (Frey and Goldring 1992)
Asterosoma isp.	In the vertical section, oval spots, may be in contact, 14–18 mm across, filled with slightly coarser material than the surrounding rock. They are interpreted as cross-sections of vertical to inclined elongated bulb-like structures tapering at both ends and spreading out from a common vertical or inclined shaft	A selective-feeding burrow of a worm (Pemberton et al. 2001), which occurs mostly in siliciclastic, rarely carbonate, typically in various shallow-marine environments, especially in the upper lower shoreface (Pemberton et al. 2001; Bromley and Uchman 2003; Pervesler and Uchman 2004)
Chondrites isp. (Figs. 7k and 8g)	Inclined, branched bars, or circular to oval spots, 0.2–1.5 mm wide, darker than the surrounding deposits. They are cross sections of downward spreading branched tunnels	A feeding deep-tier chemichnion of unknown "worms", which can burrow below the redox boundary (Fu 1991; Uchman 1999; Wetzel 2008), mostly in offshore and deeper, rarely in nearshore restricted environments (e.g., Knaust 2017; Baucon et al. 2020)
Lockeia isp. (Fig. 7d)	Vertical or steeply oblique, slightly curved, wedge-like structure, 10–12 mm high and up to 3.5 mm wide, widening upward, descending from a mudstone lamina, and penetrating through a siltstone lamina. The filling is composed of irregular stripes/patches of mudstone and siltstone	A bivalve resting trace, usually preserved as an amygdaloidal hypichnial mound (Schlirf et al. 2001; Mikuláš et al. 2013)
?*Monocraterion* isp.	In the vertical plane, a triangular structure, c. 10 mm wide, 10 mm high, which vertex is oriented downward	A domichnion of suspension feeders (Westergård 1931; Hallam and Swett 1966; Pacześna 1996; Jensen 1997; Schlirf and Uchman 2005; Stachacz 2016)
Phycosiphon incertum Fischer-Ooster 1858 (Figs. 7a–c, e, f, i, 8a, f and i)	Variable oriented, repetitive narrow U-shaped lobes, 1–15 mm wide, which in cross section show dark, single or paired centres (some show fish-hook shapes) and light mantles composed of coarser sediment. Commonly, in a diffused appearance due to soft-soupy host sediment. The large morphotype *Ph1* is 8–15 mm long and 2–3 mm wide, the medium, most common *Ph2* is 3–8 mm long and 0.3–2 mm wide, the small *Ph3* is up of 2–3 mm long and 0.1–0.3 mm wide, usually horizontally-oriented, and *Ph4* is distinguished by its occurrence in isolated patches, preferentially in fillings of *Thalassinoides* or occasionally in *Teichichnus*	Deposit-feeding trace of a small unknown vermiform organisms (Wetzel and Bromley 1994; Naruse and Nifuku 2008; Bednarz and McIlroy 2009; Wetzel 2010; Izumi 2014) in a wide-range of facies, mostly fine-grained lower shoreface and deeper, mainly siliciclastic facies (Goldring et al. 1991; Savrda et al. 2001; Pemberton et al. 2012; Callow et al. 2013). Its tracemaker colonized freshly deposited turbidites with a lot of food and well-oxygenated pore waters (Wetzel and Uchman 2001). The four morphotypes correspond to these distinguished by Rodríguez-Tovar et al. (2014)
Palaeophycus isp. (Fig. 8b)	Sub-horizontal cylindrical, lined, passively filled burrow, 2–4 mm wide, which show traces of collapsing	Burrow of variable filter-, deposit-feeding, carnivorous or omnivorous invertebrates, mostly polychaetes in a wide range of facies (Pemberton and Frey 1982; Jensen 1997; Knaust 2017)
Planolites isp. (Fig. 7h, k)	A horizontal, unlined, cylindrical tunnel, actively filled with sediment that usually differs from the surrounding. It is elliptical, sub-circular in cross sections, 2–3 mm in diameter	Locomotion and deposit feeding, actively filled burrow of variable "worms" in many marine and non-marine facies (e.g., Pemberton and Frey 1982; Fillion and Pickerill 1990, and references therein). According to Locklair and Savrda (1998), it is an open burrow that was filled with overlying sediment
cf. *Polykladichnus* isp.	Vertical to subvertical branched, unlined cylinders, which are c. 1 mm wide, crowded in clusters, which are up to 20 mm wide and up to 20 mm high. The branches diverge in the middle-upper part at acute angle	*Polykladichnus* is a domichnion mostly in marginal marine and continental deposits (Schlirf and Uchman 2005). Burrows of this pattern are produced by some nereidid polychaetes (Wang et al. 2019)
Rhizocorallium isp. (Fig. 8f)	In the vertical section: a dumbbell structure, about 60 mm wide, with lens-like, swelled terminations, which are 15 mm wide, and the thin interconnecting bar, which is 1.4–2 mm thick. In horizontal section: spreite structures, 5 cm thick with swelling at the end. The lens-like terminations are interpreted as a cross-section of the marginal tunnel	*Rhizocorallium* is produced by suspension feeders (only short oblique, retrusive forms) or deposit feeders, mostly crustaceans (Fürsich 1974; Schlirf 2000) or "worms" (Knaust 2013), mainly in in shallow marine and marginal marine deposits (e.g., Farrow 1966; Hakes 1976) and rarely in deep-sea (Uchman 1992) or even in non-marine deposits (Fürsich and Mayr 1981)

Table 1 (continued)

Ichnotaxon	Description	Interpretations and the basic references
Schaubcylindrichnus isp. (Fig. 8c)	Single, horizontal to oblique, simple tubes, ~ 2–5 mm in diameter, or rarely a bunch of subparallel tubes, displaying a white, calcareous/silty wall. In the Mochars core, trace fossil occurs in mudstones and wackestones, mainly in the upper Bifrons and Variabilis zones	Solitary funnel feeder and dwelling structure produced by enteropneusts, maldanid polychaetes, or synaptid holothurians (Nara 2006; Löwemark and Nara 2013)
Siphonichnus isp.	A steeply inclined, simple tube, c. 1.5 mm thick, which shows a darker core and thick lighter mantle. In the upper part, it may show swelling	A dwelling trace of suspension feeding bivalves (Stanistreet et al. 1980; Gingras et al. 2008; Dashtgard 2011) or a pascichnion of bivalves (Knaust 2015), common in shallow-marine and marginal-marine deposits (Pollard 1988) often related to salinity fluctuations and freshwater influx (Knaust 2015). Rare in deep-sea deposits (Krobicki et al. 2006)
Skolithos isp.	Isolated, vertical, or steeply inclined, simple, unlined cylinder, c. 1–2 mm wide and at least 15 mm long. The tube is lined with mud	Dwelling and feeding burrows of annelids or phoronids (Alpert 1974), mostly in shallow-water-high energy settings, but may also occur in deep-sea deposits (e.g., Wetzel 2007)
Teichichnus isp. (Fig. 7j)	A vertical, blade-like elongate spreite structure, 15–25 mm wide, up to 60 mm in the vertical plane. Specimens with zigzag margins in vertical cross section resemble *Teichichnus zigzag* Frey and Bromley 1985, and specimens showing only a few spreiten laminae are considered as an incipient *Teichichnus*	A feeding structure that resulted from the upward or downward displacement of a causative tube, mainly in fine-grained fully marine and brackish deposits Knaust (2017)
Thalassinoides isp. (Figs. 7c, e, f, h, l, i, 8f, i)	In the vertical section: elliptical spots up to 5–20 mm wide, or short bars of comparable size, which colour differs from the surrounding rock. In the horizontal section: branched, cylindrical burrow networks. They are usually associated with coarser (packstones-grainstones), somewhat stiffer sediments. The filling is preferentially burrowed with *Phycosiphon* (*Ph4*)	Domichnion and fodinichnion of mostly scavenging and deposit-feeder crustaceans (Fürsich 1973; Frey et al. 1978, 1984; Ekdale 1992; Bromley 1996; Schlirf 2000), in variable, presumably shallow marine environments (Frey et al. 1984; Mángano and Buatois 1991; Pemberton et al. 2001), but also in the deep-sea facies (Uchman 1995, 1998; Uchman and Tchoumatchenco 2003; Wetzel et al. 2007)
Trichichnus isp. (Fig. 7g and j)	A vertical to oblique, occasionally horizontal, straight or slightly winding, thread-like, unbranched or branched cylindrical structure, up to 1 mm in diameter	Traces of filamentous mat-forming sulfide-oxidizing bacteria (mostly *Thioploca*-related taxa,), which are able to provide an electron exchange between oxic and suboxic/anoxic sediment layers (Kędzierski et al. 2015; see also Kjeldsen et al. 2019). *Trichichnus* occurs mostly in fine-grained sediments of shallow water (e.g., Frey 1970), and deep-sea environments (e.g., Kennedy 1975; Wetzel 1981, 1983; Kotlarczyk and Uchman 2012)
Zoophycos (Fig. 8e)	A few mm thick, planar to oblique structures. The characteristic of *Zoophycos* spreiten structure is not observed in Mochras, but this is commonly the case in some fine-grained deposits (Voigt and Häntzschel 1956). The trace fossil is distributed rather evenly through the whole section, but very rare in the tenuicostatum—lower exaratum interval. Usually, only one, rarely two–three whorls appear	Fodinichnion of unknown producers, possibly sipunculids (Wetzel and Werner 1981), polychaete annelids, arthropods (Ekdale and Lewis 1991), or echiuran worms (Kotake 1992), with controversial feeding strategy (e.g., Bromley 1991; Locklair and Savrda 1998; MacEachern and Burton 2000; Bromley and Hanken 2003; Löwemark et al. 2006). Since the Mesozoic, *Zoophycos* has shown a tendency to occur in deeper environments than in the Paleozoic, from below the shelf to abyssal depths (Zhang et al. 2015)

must be compatible with occurrences of other trace fossils, representing shallower tiers and/or more oxygenated conditions. The abundance and diversity of other trace fossils disaffirms dysoxic conditions in this case.

Among other trace fossils, of note are occurrences of dwelling structures of filter-feeding organisms, building vertical structures stabilized by a mucus lining (*Skolithos*, ?*Monocraterion*, *Arenicolites*, *Siphonichnus*, cf. *Polykladichnus*). With respect to behavioural groups, it should be noted that the general abundance of suspension feeders in the Toarcian section of Mochras, although more frequent than in the Pliensbachian (Pieńkowski et al. 2021) is still low, probably because their filter apparatus can easily be plugged when the mineral suspension concentration is high (Pieńkowski 1985; Thistle et al. 1991).

All described trace fossils are important components of ichnofabrics (ichnofabric is understood as an overall texture and structure formed by bioturbation or bioerosion; see Bromley and Ekdale 1986). Constituents of ichnofabrics may be attributed to several controls and attributes, in particular to the tiering patterns and the manner of colonization (Ausich and Bottjer 1982; Taylor et al. 2003). The complete ("ideal') tiering pattern in the Mochras Toarcian section can be summarized as follows. The shallowest tier consists first of an indistinct mottling that is produced in the mixed layer by bioturbation in water-saturated soupy sediment near the sea floor, followed next by the shallow tier of *Phycosiphon* (*Ph1, Ph2, Ph3*) showing a patchy distribution. The middle tier is occupied by *Thalassinoides,* and slightly deeper *Schaubcylindrichnus*, *Planolites*, rare *Teichichnus,* and yet deeper another generation of *Phycosiphon* (*Ph4*), reworked *Thalassinoides* and rarely *Teichichnus*. The yet deeper tier is characterized by *Teichichnus* and *Zoophycos,* and the deepest one is occupied by *Trichichnus*. Rare traces (cf. *Polykladichnus, Skolithos, Arenicolites, Siphonichnus, Rhizocorallium*) usually occupy a middle tier, below *Phycosiphon* (*Ph1, Ph2, Ph3*). On the other hand, *Chondrites* occupies a deep tier. However, such a complete tiering pattern occurs rarely, and the most common tiering pattern is limited to shallowest tiers: *Phycosiphon* (*Ph1, Ph2, Ph3*), *Thalassinoides* (middle tier), with *Schaubcylindrichnus* slightly deeper, and *Trichichnus* occurring at the deepest level.

4 Discussion

4.1 Sedimentary environment, ichnodiversity, cyclicity of sedimentation

4.1.1 Sedimentary environment

The lithofacies in the Toarcian at Mochras contrast with those in other settings for the UK Jurassic (as is also the case for the Pliensbachian). For example, the Toarcian in the Cleveland Basin, some 300 km to the NE of Cardigan Bay, is represented by organic-rich (black) shale up to late Bifrons Zone age, known as the Mulgrave Shale (formerly the Jet Rock), similar to the Schistes Cartons of France and Posidonia Shale of Germany (Jenkyns 1988; Atkinson et al. 2022). These strata were deposited in a restricted shelf basin (Powell 2010) that was episodically affected by storm processes (e.g., Kemp et al. 2018). Higher levels within the Cleveland Basin Toarcian are clearly deposited in a storm-dominated shoreface setting (e.g., Hesselbo and King 2019).

Based on sediment transport processes, the action of two different types of deep-water currents and their depositional products have been recognized in the Mochras section, namely contourite drift facies produced by along-slope contour currents (see Pieńkowski et al. 2021 for the Pliensbachian part of the section) and turbidite deposits created predominantly by downslope sediment density flows (Xu et al. 2018a—Exaratum Subzone, Serpentinum Zone, of the Toarcian section). Xu et al. (2018a) illustrated few cm-scale sharp-based beds in the T-OAE interval described as turbitites. However, fining upwards of these beds is not gradual, with coarser intercalations sharply separated not only from below, but also from above without continuous transition; therefore, these beds may alternatively represent repeated intensifications of along-slope currents. It is also possible that sediments of distal turbidites could occasionally have been "pirated" by contourite currents (Gong et al. 2017; Rodríguez-Tovar et al. 2019a, b), and such a situation could also have occurred in Mochras.

Apart from this T-OAE interval, the Toarcian section in Mochras does not reveal any features of typical turbidites. The silty-sandy beds and laminae in the studied section show no systematic vertical grading or stacking of structures, such as those recognized in the Bouma (1962) intervals. The Mochras section overall records continuous sedimentation with structures characteristic of current traction, controlled by fluctuation of their speed; therefore, deposition by turbiditity currents was unlikely. In addition, turbidites are primarily bioturbated from the top (e.g., Uchman and Wetzel 2011) and the uppermost layers of a turbidite exhibit total bioturbation, which decreases with depth as lamination and cross bedding appear. In contrast, contourites typically exhibit more continuous and uniform bioturbation, which appears throughout the entire contourite bed; this situation is typical for both the Pliensbachian and Toarcian of Mochras. However, the variability of ichnofabric pattern in contourites may depart from this typical picture (Rodríguez-Tovar et al. 2019a, b, 2022).

Interpretation of a wide spectrum of bathymetry and occurrences of contourite currents is recognized, i.e.

everywhere the sea floor had a considerable relief, commonly of more than a hundred metres amplitude, comprising moats, drifts, mounds and channels (e.g., Bein and Weiler 1976; Surlyk and Lykke-Andersen 2007; Esmerode et al. 2008; Van Rooij et al. 2010; Rebesco et al. 2013), although the definition of Faugeres and Stow (2008) is also applied, according to which the term contourite should be generally used for sediment accumulated in relatively deep water (markedly deeper than c. 200 m-deep shelf platform) and deposited or significantly reworked by stable currents.

The deposits in Mochras can be classified as mixed siliciclastic-calcareous/biogenic contourites, the most frequent contourite facies in the modern oceans (Fagueres and Mulders 2011). In less bioturbated sections of Mochras, primary sedimentary structures are visible and are mostly represented by current structures such as planar parallel lamination, low angle cross-lamination, starved ripples, in places erosive bases, and gradational normal grading bed transitions (Fig. 5a), like cases studied by Shanmugam (2000) and Knapp et al. (2017). Stagnant conditions or very slow currents allowed vertical settling of the suspended particles from the nepheloid layer (Ewing and Thorndike 1965) producing mottled mudstone (Fig. 8d), or laminated mudstone-claystone (Figs. 7a and 8h), where the grain-supported laminae are interpreted to be the result of very weak contour currents that winnowed out clay-sized sediment (e.g., Shanmugam 2000).

Higher bottom current velocities led to deposition of silt or sand layers with planar or low-angle cross-bedding, produced by bedload transport (Figs. 5c, d and 7d) and periodically these currents were strong enough to erode older sediments and carry coarse-grained sediments, including clay intraclasts and pebbles (Fig. 6). Compared to the Pliensbachian (Pieńkowski et al. 2021), visible plant remains are more frequent (see also Ullmann et al. 2021) and indicate more phytodetrital pulses in connection with fluvial discharges in the hinterland, which possibly could have led to acidification (Müller et al. 2020) and intermittently reduced salinity of sea water (Dera and Donnadieu 2012), both adding (along with the Toarcian rise in pCO_2; see Hermoso et al. 2009) to collapses of the carbonate factory (Bodin et al. 2023), suggested particularly for the Tenuicostatum Zone to Exaratum Subzone interval (Fig. 2a). Relatively weaker bioturbation can be attributed to oxygen depletion or high sedimentation rate (Stow and Fagueres 2008); assuming rather stable sedimentation rate, weaker bioturbation is here largely attributed to decreasing circulation and oxygenation. One should bear in mind that strong bottom currents (Fig. 6) also do not favour preservation of biogenic structures (Tucholke et al. 1985).

Fully developed bigradational intervals in the Mochras section (Fig. 5) correspond to a standard contourite sequence (Faugeres et al. 1984; Stow and Holbrook 1984; Stow et al. 2002; Huneke and Stow 2008; Rodríguez-Tovar and Hernandez-Molina 2018), a continuation of the situation for the Pliensbachian (Pieńkowski et al. 2021). The standard contourite model was enhanced by introduction of interval divisions (C1 to C5; Stow et al. 2002; Stow and Faugères 2008, their Fig. 13.9) and recognition of variations within partial contourite sequences (Rebesco et al. 2014; Shanmugam 2017), corresponding to observations in the Mochras profile (Figs. 4 and 5) where most frequent vertical sequences consist of lithofacies types 1/2–3–4–5–6 (in coarsening-upward order) and subsequent fining-upward couplet composed of 5–4 lithofacies types. The fining-upward phase of the fully developed cycle is usually thinner and incomplete. In places, these sequences are interrupted by erosional surfaces and coarse sediments, including conglomerates (lithofacies type 7; Fig. 6). Periods of strong currents marked by erosional surfaces and coarser material, pointing to intermittent non-deposition/erosional periods, appear first in the late Falciferum Subzone of the Serpentinum Zone, and occur mostly in the late Bifrons Zone, Variabilis-Thouarsense transition, and the late Levesquei Subzone (Fig. 2a, b). In such cases the bigradational grading cycles are often incomplete, lacking their upper parts (top-cut-out cycles; see Fig. 5a). The depositional rate at Mochras during the Toarcian remained generally stable and relatively high, but the sections mentioned above show condensation (Figs. 2a, b, 5 and 6).

4.1.2 Ichnodiversity

Occurrences of trace fossils also show a cyclic character, more or less corresponding with lithological changes and sedimentary cycles. At one end of a spectrum is the domination of opportunistic, r-selected *Phycosiphon*, diffused shape of trace fossils, indications of soft-bottom conditions (Fig. 7f), mostly simple tiering, and scarcity of highly specialized K-selected forms, all indicating a generally stressful environment (e.g., Ekdale 1985), which was probably caused by high sedimentation rate associated with unstable substrate and intermittent benthic food availability, interrupted by transient oxygen-depleted, more stagnant conditions.

The other end of the spectrum is characterised by higher substrate stability (stiffer conditions), lower sedimentation rate, continuous delivery of suspended nutrients by currents (often adsorbed onto suspended clay minerals – Mayer 1994; Thistle et al. 1985), and usually fairly good oxygenation of the bottom, leading to more complex tiering under equilibria (Taylor et al. 2003). A high degree of bioturbation is characteristic

for contourites due to additional food supply (the vertical particle flux is supplemented by lateral current-carried supply) and faunal abundance (Suess 1980; Wetzel et al. 2008). In agreement with Caswell and Frid (2017), changes in community composition are usually linked to local redox conditions, whereas changes in populations of r-selected opportunists are driven by primary productivity.

4.1.3 Cyclicity of sedimentation and spectral analysis of ichnological data

Four orders of cycle duration are determined based on visual inspection of the sedimentary succession. A 4th-order cyclicity is interpreted as a superposition of precession (c. 20 kyr) and obliquity terms (c. 38 kyr, Waltham 2015). Precession and obliquity cycles are hardly distinguishable from each other in direct observation, but are identified discretely by spectral analysis. The 3rd and 2nd order cycles are identified with short eccentricity (c. 100 kyr) and long eccentricity (c. 405 kyr), respectively (Kent et al. 2018). A 1st-order cyclicity is attributed to eccentricity modulation of the c. 2.4 Myr period, which is caused by secular resonance between Earth and Mars (Hinnov 2000; Laskar et al. 2004, 2011).

As described previously for the Pliensbachian (Pieńkowski et al. 2021), the distinction of cycles in the Mochras Toarcian is based mainly on grain size and ichnological features and their lower boundaries are placed in the fine-grained, mottled, or laminated mudstone (lithofacies 1 and 2; see Fig. 4). Both the fully developed (bigradational), and the incomplete lithological couplets with their ichnological content, constitute the 4th order cycles, basic 'building blocks' of the hierarchical order of cycles in Mochras (Figs. 2a, b and 5). Commonly, in these cycles, meiofauna mottling (undulated bedding) appears first, followed by colonization of *Phycosiphon* (*Ph3*) as the first recognizable trace fossil, then *Ph2* and other trace fossils return. These 4th order cycles are arranged in higher hierarchical successions (3rd order cycles), usually containing four, locally five, 4th order cycles. As every 3rd order cycle commences with the 4th order cycle, the 3rd order cycles start from meiofauna mottling and *Ph3*. *Schaubcylindrichnus*, occasionally accompanied by *Planolites*, tends to appear at the tops of these cycles. In many cases *Zoophycos* can be found in the middle, and occasionally K-selected (equilibrichnia) forms, such as *Skolithos, Arenicolites* and *Siphonichnus* (dwelling/suspension feeders' structures), bivalve resting tracks *Lockeia*, larger deposit feeder structures *Rhizocorallium*, and *Chondrites* (chemichnion), appear at boundaries of these cycles.

Next, 2nd order cycles are composed of four 3rd order cycles. Sixteen out of 24 of the 2nd order cycles show occurrences of K-selected (equilibrichnia) forms (such as *Skolithos*, *Arenicolites*, *Monocraterion*, *Siphonichnus*, *Rhizocorallium* and *Chondrites* at its boundaries, pointing to more stable conditions. Both 2nd and 3rd order cycle boundaries show sharp-walled, uncompacted, passively filled burrows that point to condensation/non-sedimentation (Fig. 8i).

Erosional surfaces, commonly associated with coarse-grained sediments, always indicate sedimentation breaks and play an important role in the interpretation of the boundaries of the cycles. Usually, boundaries of the 2nd or occasionally 3rd order cycle are placed at these surfaces. High velocity contourite currents are known to generate erosional surfaces and contourite lag facies, resulting from winnowing, reworking processes and hiatuses (Faugerez and Mulder 2011). In Mochras, the lag facies contain a large range of grain sizes and compositions, forming irregular centimetre-thick to metre-thick beds of poorly sorted sediments, mainly coarse sands, gravels, and pebbles or rip-up clasts (Fig. 6).

The highest, 1st order, cycles are composed of six 2nd order cycles. The beginning of the Toarcian sequence of these cycles is anchored at the Pliensbachian-Toarcian boundary, where the succession of four previous 1st order cycles of the latest Sinemurian to Pliensbachian age ends (Pieńkowski et al. 2021). These 1st order cycles in the Toarcian differ from those observed in the Pliensbachian, mainly because a regular, short- and long-term cyclicity of $CaCO_3$ content (Ruhl et al. 2016; Pieńkowski et al. 2021) disappears in the Toarcian, making the $CaCO_3$ content generally of less use in reconstructing the cyclicity. Reduced $CaCO_3$ content can be attributed to environmental change that occurred at the beginning of the Toarcian. In a similar fashion to the Pliensbachian 1st order cycles, the greatest ichnodiversity tends to appear in their middle parts. Higher ichnodiversity usually also coincides with condensation (Fig. 2a, b). This interpreted ~ 2.4 Myr cyclicity retains its regularity throughout the entire Pliensbachian–Toarcian section of Mochras, although Charbonnier et al. (2023) postulated much shorter cyclicity (~ 1.6 Myr) for the Sancerre core in Paris Basin—see discussion below.

Because generally the whole Toarcian in Mochras is dominated by *Phycosiphon*, any lack of this morphotype is noteworthy, as it indicates an exceptionally unfavourable environment, most likely associated with stagnation and oxygen depletion. Of particular note is the fine-grained interval between 823 and 868 mbs, mostly Tenuicostatum Zone, dominated by mudstone and claystone, with significantly reduced $CaCO_3$ content, frequent siderite occurrences (Xu et al. 2018a) and a marked foraminiferal biotic crisis (Reolid et al. 2019). Here, *Phycosiphon* is reduced in frequency, and other trace fossils are very scarce, while *Trichichnus* and undulated bedding

are prolific. Only for the middle of this interval (~ 838 to ~ 853 mbs) can some intermittent improvement of bottom life conditions be inferred, indicated by less continuous occurrences of *Trichichnus*, brief re-appearances of *Phycosiphon,* and presence of cf. *Polykladichnus* and *Chondrites* (Fig. 2a). This slight recovery is also observed in foraminiferal assemblages (Reolid et al. 2019).

Less severe ichnological crises are noted in the Thouarsense-Dispansum zones with *Trichichnus* occurrences and diminished ichnodiversity. Here, *Phycosiphon* scarcity is also observed although, compared to the earliest Toarcian, less pronounced. Relatively abundant *Trichichnus* occurrences in the mid-Pseudoradiosa Zone are accompanied by appearances of other diversified trace fossils; thus, this section can be regarded as not affected by oxygen depletion. The Bifrons and Variabilis zones generally represent well-oxygenated intervals, shown by common occurrences of *Thalassinoides*, *Schaubcylindrichnus*, *Teichichnus* and other trace fossils, including domichnia; only over depths 710–720 mbs is a slight decrease in oxygenation inferred, marked by decreased ichnodiversity and presence of *Trichichnus*.

Smoothed curves of particular ichnotaxa occurrences juxtaposed with smoothed Zr/Rb, Ti/Al, Si/Al, Ca, TOC, $\delta^{13}C_{TOC}$, and gamma ray records reveal a high degree of similarity (Fig. 3). The relationship of particular trace fossil occurrence curves to each proxy record is, to some extent, disparate, and the parallelism of respective curves varies through the succession. Nonetheless, the outlines of several curve crests are visually coherent, and the phase difference is insignificant given the timescale. Most notably, the T-OAE-negative CIE has coincident expressions in the records of all analyzed ichnotaxa. The Zr/Rb record, a proxy for silt/clay ratio, displays resemblance to the highest number of ichnotaxa occurrences (five; Fig. 3), and the *Thalassinoides* occurrence curve resembles the highest number of proxy records (five). The best visual coherence appears to occur between the curves of the following: Zr/Rb—*Phycosiphon* type 3, *Thalassinoides* and *Planolites*; Si/Al—undulated bedding; Ca content—*Thalassinoides* and undulated bedding; TOC content—*Schaubcylindrichnus*.

Interpretation of cyclicity and resulting calculation of time based on these cycles attributed to certain orbital cycles becomes more complex in sections with erosional surfaces, associated with inferred hiatuses in sedimentation, resulting in less regular sedimentation rate and cyclicity. It is reasonable to interpret that much of the lost time is represented at the erosional/hiatal surfaces. It is difficult to say how long lasting were time intervals of non-sedimentation, or how deep was erosion of previously deposited sediments. In such cases, the 1st order (~ 2.4 Myr) cycles can provide some time frameworks, allowing for approximate adjustment of the 2nd and 3rd order cycles to the ~ 2.4 Myr duration of 1st order cycles. This is particularly important in the Toarcian above the Serpentinum Zone, where most erosional/hiatal surfaces with coarser sediments occur, usually concentrated in the middle parts of the 1st order cycles (Fig. 2a, b).

For numerical cyclicity (spectral) analysis only frequently occurring trace fossils can be used. *Phycosiphon incertum* is by far the most common trace fossil in the Mochras section. As it is represented by four distinct morphotypes (*Ph1, Ph2, Ph3, Ph4*), they are treated separately for analysis of cyclicity (in the Toarcian *Ph2* and *Ph3* were used). *Thalassinoides*, *Schaubcylindrichnus, Planolites,* and *Trichichnus* are also frequent enough to be used for analysis of cyclicity as well. Other ichnotaxa are not frequent enough for spectral analysis, although their cyclic appearances yield useful information concerning a more general hierarchy of cycles. Additionally, lamination and undulated bedding can be used for spectral analysis.

The runs test results indicate the non-random distribution of either trace fossil, lamination and undulated bedding occurrences in the studied sedimentary succession (Additional file 2), demonstrating the advisability of time series analysis. Absolute values of all computed Z-scores are within the critical region of > 1.96, which allows rejection of the null hypothesis of the data randomness at the 95% confidence level.

The peak values of the Walsh power-spectra (Fig. 9) correlate to the calculation-based expected duration of the orbitally forced periodicities (Table 2). The resultant spectral peaks (Fig. 9) have estimated time values assigned as explained in Sect. 2. Component frequencies of precession, obliquity and short eccentricity, as well as beat frequencies, are present in the resultant spectra besides the main terms (Tiwari 1987; Negi et al. 1993). The longer the periodicity, the more prone it is to be blurred by instantaneous changes in the sedimentation rate. Besides, shorter-term periodicities can be recorded with higher precision than these longer-term, as a larger number of them are contained within the studied time series.

Either one or more spectral peaks in the sequency range of circa 0.9–1.2 cycles/m are reflected by most of the analysed time series, with the exception of *Trichichnus* (Table 2). These prevalent, albeit relatively low-power peaks are interpreted as precessional terms corresponding to the visually determined 4th order cycles. *Schaubcylindrichnus* occurrences reflect the most (three) component terms in the range of precession, which in this case are characterised by spectral power on par to the other periodicities.

Table 2 Spectral peak values recognized in the present study against the background of calculated present-day component orbital periodicities

Phycosiphon **morphotype *Ph2* [kyr]**	***Phycosiphon*** **morphotype *Ph3* [kyr]**	***Thalassinoides*** **[kyr]**	***Schaubcylindrichnus*** **[kyr]**	***Planolites*** **[kyr]**	***Trichichnus*** **[kyr]**	**Lamination [kyr]**	**Undulated bedding [kyr]**	**Calculated orbital periods [kyr]**	
					155–174	132–148		173	Obliquity AM
104–117	108–121		115–129	111–125				112	Eccentricity bands
		81–91					75–84	95	
			66–74.2					59–64	Combined effect
	36.2–40.7		39.9–44.9		42.6–47.9			40–42	Obliquity bands
							35.3–39.7	37.5	Main obliquity term (Toarcian)
29.8–33.4	25.9–29	24–27	35.6–40	25.7–28.9		29.6–33.3		29–30	Obliquity bands
26.8–30.1	21.3–24		22.2–25			19.1–21.5	19.9–22.4	22–24	Precessional bands
19.9–22.4		18–20.2	19.6–22	17.5–19.7		17–19.1		19	
			17.7–19.9					16–17	

Present-day component orbital periodicities after Berger (1977); main obliquity term for Toarcian taken from Waltham's (2015) Milankovitch Calculator; obliquity amplitude modulation (AM) after Hinnov (2000)

Periodicities in the range of either main obliquity term (*Phycosiphon Ph3* and undulated bedding) calculated for the Toarcian (Waltham 2015), or theoretical component obliquity terms (remaining time series) are distinct in all Walsh spectra, even though obliquity is not readily distinguished visually in the sedimentary succession. Periodicity of c. 28 kyr is observed in the occurrences of *Phycosiphon* (*Ph2* and *Ph3*) and *Planolites*, which can probably be identified with the shortest component term of obliquity (Tiwari 1987; Laskar et al. 2011). Presumably, the peak near the 0.31 cycles/m value displayed by *Schaubcylindrichnus* occurrences (Fig. 9) can be associated with the combined effect of obliquity and precession, as proposed by Berger (1977).

Peaks interpreted as short eccentricity (3rd order) terms are the most intensely (high-power) represented in the spectrograms (Fig. 9). Periodicities in the range of c. 105–120 kyr recorded by *Phycosiphon Ph2* and *Ph3*, *Schaubcylindrichnus* and *Planolites* (Fig. 9) can be identified as the longer component term (c. 112 kyr) of short eccentricity cycles, presumably reflecting the 3rd order cycles distinguished in the sedimentary and ichnological record (Fig. 2a, b). In addition, ~ 90 kyr periodicity displayed by *Thalassinoides* can be interpreted as the shortest eccentricity component term (~ 95 kyr).

Trichichnus occurrences record also the periodicity of the ~ 170 kyr term, which likely can reflect a cyclicity of c. 150–170 kyr, also present in the Pliensbachian of Mochras, and there preliminarly regarded as non-astronomical (Pieńkowski et al. 2021). However, this cyclicity could be associated with the amplitude modulation (AM) of the obliquity (Hinnov 2000). Such AM 173 kyr periodicity was hitherto detected in the sedimentary record by the means of time series analysis by Laurin et al. (2015), Boulila et al. (2018), Vahlenkamp et al. (2018) and Huang et al. (2021).

The peak clusters present in the leftmost parts of the *Planolites*, *Thalassinoides* and *Trichichnus* spectrograms may be associated with 2nd order ~ 405 kyr cycles (registered by recurrent appearances of *Skolithos*, *Siphonichnus*, *Arenicolites*, and *Chondrites*, which were not included in the spectral analysis due to their low frequency). However, this remains a presumption due to spectral resolution of spectra below the sequency values of 0.1 cycles/m being inadequate to confidently interpret these peaks in the time domain.

The most complete representation of orbital periodicities is reflected by both *Phycosiphon* morphotypes, *Thalassinoides, Schaubcylindrichnus and Planolites* (Fig. 9) which clearly display the frequencies of the short eccentricity terms (~ 95 and 112 kyr), obliquity terms (~ 29 and ~ 40 kyr) and precessional terms (~ 17–25 kyr). Spectra of both *Phycosiphon* morphotypes show a good congruence, especially considering an interpreted longer component term of short eccentricity. In the case of *Phycosiphon Ph2*, it can be supposed that evident

periodicities associated with either 4th or 3rd order cycles are derivative of periodic short non-occurrences of this pervasively occurring trace fossil. Interestingly, *Trichichnus* occurrences seem solely to reflect periodicities related to obliquity and its AM frequency.

Longer-term 'grand cycles' which are not included in spectral analysis, are characterized by a gradually growing and subsequently falling *Phycosiphon* frequency and general ichnodiversity. Judging by the duration of ~ 100 kyr and ~ 405 kyr eccentricity cycles, these longer-term eccentricity "grand cycles" would be of duration c. 2.4 Myr, corresponding to the period of around 2.4 Myr eccentricity modulation related with Mesozoic greenhouse sequences, caused by Earth–Mars secular resonance (Hinnov 2000; Laskar et al. 2004, 2011; Martinez and Dera 2015). Whereas individual repetitions of the ~2.4-Myr cycle range from 2.0 to 2.9 Myr in the Cenozoic (Pälike et al. 2006), cyclostratigraphic studies suggest that this period fluctuated between maximal values ranging from ~1.3–3.3 Myr during the Mesozoic (Ikeda and Tada 2013, 2020). Indeed, the periodicity of grand eccentricity cycles prior to 50 Ma remains uncertain. Charbonier et al. (2023) postulated a chaotic behaviour of the Solar System and ~ 1.6 Myr Earth-Mars resonance cyclicity (instead of ~ 2.4 Myr) for the Early Jurassic, based on the Sancerre-Couy core (Paris Basin). However, Wu et al (2022), while also suggesting transient chaotic behaviour of the Solar System in the Late Cretaceous of the Songliao Basin (China), revealed evidence for two chaotic secular resonance transitions in the orbital motions of Earth and Mars, involving the orbital eccentricity modulations of 2.4 Myr and 1.2 Myr cycling, without indication of ~ 1.6 Myr cycling. We support the ~ 2.4 beat (Martinez and Dera 2015), because the observed general ichnological cycles, which are built on well-established hierarchy of sub-cycles, are much less compatible with the ~ 1.6 Myr duration of grand orbital cycles of Charbonier et al. (2023) than with the ~ 2.4 Myr cycles (Fig. 2a, b).

The existence of yet longer cyclicity, ~ 7–8 Myr eccentricity (Martinez and Dera 2015; Pieńkowski et al. 2021; Charbonier et al. 2023) is supported, based on two possible such cycles in the combined Pliensbachian-Toarcian section.

4.2 Toarcian deep sea current circulation

Oxygen deficiency and resulting decline in ichnodiversity can be attributed to the diminishing current intensity, but also to other related or independent causes, including high organic productivity and sea level. The earliest Toarcian crisis that had begun already in the latest Pliensbachian was exceptional in its severity (Xu et al. 2018a; Reolid et al. 2019; Pieńkowski et al. 2021; Bodin et al. 2023). Most likely, the benthic crisis was associated with severe stagnation of circulation through the Laurasian Seaway (and the Cardigan Bay Strait) at that time (Van Schootbrugge et al. 2019). Thermohaline circulation driven by density differences between water masses due to variations in water temperature and salinity is still regarded as the major driving force of contourites (McCave 2008; Faugeres and Mulder 2011; Rebesco et al. 2014). The biogenic input from shallower zones, likely carbonate platforms, was less marked than in Pliensbachian, and was replaced by a stronger siliciclastic input, which also carried more floral debris and possibly connected to acidification (Xu et al. 2018a, b; Müller et al. 2020)—although $\delta^{44}/^{40}$Ca and $\delta^{88}/^{86}$Sr records do not support acidification (Li et al. 2021). Bottom currents carried in suspension a considerable amount of particulate organic matter, supplying food to deep-marine benthic organisms (Thistle et al. 1985). As for the Pliensbachian, it is proposed here that the deep-water circulation in the elongated, NE-SW trending Cardigan Basin (Fig. 1) was forced by enhanced bottom-water circulation, i.e. cooler and denser waters flowing with changing velocity from the Boreal Sea, around the Shetland Platform-Scottish Landmass island, towards the south, to the Peri-Tethys/proto-Atlantic, approximately parallel to the bathymetric contours of the margin of the Welsh Platform (Fig. 1).

Interpretations of circulation (Bjerrum et al. 2001; Dera et al. 2009; Dera and Donnadieu 2012; Ruvalcaba Baroni et al. 2018) point to the predominant southward flow from the Arctic into the Tethys through the Laurasian Seaway during the Early Jurassic. The Cardigan Bay Strait, linking cooler and shallower waters of the Boreal Sea with warmer and deeper waters of Peri-Tethys (Fig. 1), would then have been situated to sustain a continuous (persisting for up to millions of years and over large areas—Shanmugam 2008, 2017) thermohaline-driven contour current circulation between these two marine realms (Pieńkowski et al. 2021). These invigorated flow conditions were punctuated by times of sluggish circulation or stagnanation characterised by loss of ichnodiversity and *Phycosiphon* crises (usually also by mass *Trichichnus* occurrences), as well as appearance of undulated bedding. These intervals occur in the Tenuicostatum Zone through to earliest Exaratum Subzone age strata and, to a lesser extent, in the latest Thouarsense Zone to Dispansum Zone.

This sluggish circulation is associated with climate warming under high atmospheric pCO_2, when the Laurasian Seaway was influenced by strong clockwise circulation in the Tethys, which brought warm saline waters onto European shelves and then diminished the effects of flow from the north through the Laurasian Seaway (Ruvalcaba-Baroni et al. 2018). In the same time, loss of

polar sea ice and stronger high-latitude continental runoff rates could further result in a weakening of thermohaline circulation, and bottom water oxygen depletion also in deep marine settings (Dera and Donnadieu 2012; Van de Schootbrugge et al. 2019).

For the Pliensbachian-Toarcian boundary interval, this scenario is applicable, as a warming pulse is postulated (associated with initial stage of the Karoo magmatism; Dera et al. 2009; Pieńkowski et al. 2016; Ruebsam et al. 2020). However, for the remaining part of the Tenuicostatum Zone many authors (e.g., Brandt 1986; McArthur et al. 2000; Guex et al. 2001; Suan et al. 2010; Dera et al. 2011; Korte and Hesselbo 2011; Krencker et al. 2014; Korte et al. 2015; Ruebsam et al. 2020; Ullmann et al. 2020) suggest overall persistent cool conditions, which should (according to the thermohaline-oceanic circulation mechanism) cause enhanced circulation—which is not observed in Mochras, where stagnation dominates. Only in a short interval between ~ 838 and ~ 853 mbs, is there a slight improvement of bottom conditions (confirmed also by foraminiferal assemblage; see Reolid et al. 2019), which could be associated with somewhat increased current intensity, possibly caused by a transient cooling, but this signal is weak.

Concerning the circulation problem, even more intriguing is the To-CIE interval, well known to be associated with the most severe carbon-cycle disruption, high pCO_2 and extreme greenhouse conditions, which should cause even stronger diminution of southward flow and extreme sea-floor current stagnation at that time; instead, shortly after the beginning of the To-CIE (in our calculation ~ 200 kyr), the deep-sea circulation significantly accelerated. Only at the beginning of To-CIE did sluggish circulation and oxygen depletion persist, which is indicated by the continued *Phycosiphon* crisis and common occurrences of *Trichichnus*. For the remaining part of the To-CIE event, certainly from its climax (~ 820 mbs), gradually improving circulation can be interpreted. This is recorded by common current-generated structures (pin-stripe current lamination, occasionally ripple-cross lamination), some sharp boundaries and coarser sediments, and gradual return of more diversified trace fossils, such as *Phycosiphon*, *Thalassinoides*, *Schaubcylindrichnus*, *Planolites*, *Lockeia*, *Asterosoma*, *Skolithos* and *Rhizocorallium,* and concomitant demise of *Trichichnus* (Fig. 2a). The recovery is also visible in the foraminiferal assemblage (Reolid et al. 2019).

It is noteworthy that anoxia was suggested by some geochemical indices to be coincident with this 'recovery' phase of the To-CIE: Xu et al. (2018a) reported trace amounts of the biomarker isorenieratane (with slightly elevated gammacerane indices) at two horizons (811.66 mbs and 819.10 mbs) at and just above the peak of the To-CIE. Isorenieratane is a pigment of photosynthetic green sulphur bacteria, Chlorobiaceae, that is regarded as an indication for photic zone euxinia in the water column (Koopmans et al. 1996). We investigated these horizons in detail, finding that they contain bioturbated mudstones, either by meiofauna (Fig. 8e), or more distinctly by *Phycosiphon incertum* type 2 (Fig. 8h). This means that anoxic to euxinic conditions in the photic zone would not necessarily have affected the seafloor in Mochras, which was continuously oxygenated by deep-sea bottom currents. This observation is of more general significance, suggesting that geochemical indices (even if correctly pointing to certain conditions in a shallow-water column) may not always indicate euxinic bottom conditions, because deep-sea currents could deliver enough oxygen to sustain life there, even if the shallow-photic zone was anoxic. However, a scenario of bottom re-oxygenation (to the degree required by trace makers) and overprinting by bioturbation of sea floor that had been previously affected by anoxia is also possible—although this would still point to the short and transient nature of any oxygen crisis and, given the water depth and muddy productive nature of the water column, the sea-floor is unlikely to have been in the euphotic zone.

Observed lithological and ichnological fluctuations in the Toarcian are thus associated with alternating periods of vigorous currents and more stagnant conditions on various timescales, while nutrient availability seems to have been relatively stable and sufficient all the time (as shown by the TOC content; see Xu et al. 2018a) and played a subordinate role in setting ichnological trends. Hierarchical cyclic successions observed both in lithology and ichnology indicate that orbital forcing was still the main controlling mechanism. However, at the beginning of the Toarcian, the lithological and ichnological appearance of these cycles became different, which can be linked to non-orbital, intrinsic Earth mechanisms leading to prolonged ichnological crisis in the Tenuicostatum Zone. More generally, it is also observed that compared to the Pliensbachian, the energy of contour currents in the Toarcian (after the Tenuicostatum Zone) was overall higher, temporarily producing marked erosional surfaces and carrying coarser sediment, which collectively resulted also in less regular thicknesses of sedimentary packages corresponding to individual ~ 100 and ~ 405 kyr cycles (although the 1st order cycles retained approximately stable thicknesses, which point to a generally stable average sedimentation rate in a longer period of time). Although there is no clear correlation between the organic matter carbon isotopes and observed higher energy of currents, there is a return to generally lighter values of $\delta^{13}C$ from the middle part of the Bifrons Zone.

Of note also is the repetition of the two fine-grained intervals characterized by particularly sluggish circulation, impoverished ichnodiversity (including the *Phycosiphon* crises), and abundance of *Trichichnus*: the lower one of latest Spinatum Zone to Tenuicostatum Zone age, and the upper one belonging to the Thouarsense and Dispansum zones. These intervals are separated by ~ 7.5 Myr in Mochras. A similar mega-cycle was observed in the Pliensbachian section (Pieńkowski et al. 2021), and comparable long cycles have also been hypothesised by Martinez and Dera (2015) and Charbonnier et al. (2023) and tentatively identified with a very long eccentricity term.

4.3 Climate changes and carbon cycle disturbances: impact on deep-sea circulation and orbital forcing

Two intrinsic Earth events should be considered carefully in terms of their influence on the Toarcian hemipelagic sedimentation in Mochras. The first was the Pliensbachian-Toarcian (Pl-To) boundary event, characterized by a CIE that is globally documented and linked to the initial phase of volcanism in the Karoo Province; the second event with profound impact on the marine and continental environment was the To-CIE (also known as the Jenkyns Event), dated to the latest Tenuicostatum Zone to Exaratum Subzone of the Serpentinum Zone, linked to large-scale eruptions in the Karoo-Ferrar basaltic province and associated with a rapid increase in atmospheric pCO_2 levels and average atmospheric and marine temperatures (see e.g., Hesselbo et al. 2000, 2007; Littler et el. 2010; Hesselbo and Pieńkowski 2011; Bodin et al. 2016, 2023; Pieńkowski et al. 2016; Fantasia et al. 2018; Xu et al. 2018a; Ruebsam et al. 2020; Al-Suwaidi et al. 2022; Ruhl et al. 2022).

It is important to understand how these major environmental changes, indicated by disturbances in the carbon cycle, affected the deep-sea circulation. For a long time (since the Sinemurian) this circulation was controlled in a stable way by orbital forcing, expressed in cyclic fluctuations of southward flowing thermohaline contour currents in the Cardigan Bay Basin, particularly expressed in long-term trends governed by grand eccentricity (~ 2.4 Myr) cycles (Pieńkowski et al. 2021). Notably, Charbonnier et al. (2023) postulated shortened long-period cyclicities of ~ 1.6 and ~ 3.4 Myr in Early Jurassic orbital periods, possibly reflecting the chaotic orbital motion of the inner planets (likely corresponding to the Cenozoic 2.4 Myr and 4.7 Myr eccentricity terms). This is incompatible with our interpretation even if the 7–8 Myr very long eccentricity cycle and the Toarcian duration postulated both by Charbonier et al. (2023) and by us are in agreement. Possibly, in Mochras we would have to deal with the mutual modulation of the two cyclicities indicated by Charbonier et al. (2023), giving approximately the resultant cyclicity of 2.4–2.5 Myr observed in Mochras.

The 2.4 Myr cyclicity in the present work was directly observed in the core by visual scrutiny of the variability of sedimentological and ichnological parameters. In turn, long-period cyclicities were detected by Charbonier et al. (2023) based solely on the numerical spectral decomposition of magnetic susceptibility time series from the Sancerre-Couy borehole, Paris Basin, France. Such spectral techniques reveal component frequencies of basic orbital periodicities that directy affect the sedimentary record. Importantly, Pliensbachian grand orbital cycles in Mochras (Pieńkowski et al. 2021), put together on an interpreted 405 kyr cyclicity based on $CaCO_3$ cyles (Ruhl et al. 2016), clay minerals (Deconinck et al. 2019), $\delta^{13}C$ (Storm et al. 2020) and ichnology-sedimentology (Pieńkowski et al. 2021) also show prevalence (despite some discrepancies) of ~ 2.4–2.5 Myr cyclicity. This arrangement, based on direct ichnological and sedimentological observation, persists into the Toarcian at Mochras. Therefore, we favour effective influence of ~ 2.4–2.5 Myr cyclicity on sedimentary processes in Mochras, because adoption of the ~ 1.6 Myr cyclicity postulated by Charbonier et al. (2023) is less comparable to observed long-term sedimentary and paleoecological trends observed both for the Pliensbachian (Pieńkowski et al. 2021) and the Toarcian (this study). The possibility of blurring and distortion of orbital cyclicity by autocyclic depositional processes, or tectonic processes, particularly in shallower epicontinental environments such as at Sancerre, should not be totally ruled out in that context.

As shown by our data from the Toarcian of Mochras (Fig. 2a, b), the effects of orbital forcing were no doubt also influenced by the palaeoceanographic, palaeoenvironmental and tectonic factors. The picture obtained differs from surrounding epicontinental seas, showing also more complicated mechanisms of oceanographic processes, as a result of mutual influence of orbital forcing and non-orbital changes related to large-scale volcanism and climatic/environmental disturbances. The mechanism linking sluggish deep-sea circulation with climate warming, proposed by Dera and Donnadieu (2012), Ruvalcaba Baroni et al. (2018) and Van Schootbrugge et al. (2019), suggested for the Sinemurian–Pliensbachian section (Pieńkowski et al. 2021), appears to be still valid for most of the Toarcian in Mochras, but fails to explain changes that occurred in the earliest Toarcian (Tenuicostatum–Exaratum interval). Severity and continuity of the latest Pliensbachian to earliest Toarcian stagnation and benthic crisis probably occurred during transition from supposed icehouse to greenhouse conditions (Dera and Donnadieu 2012; Krencker et al. 2014; Bodin et al. 2023)

and from sea-level lowstand to marked sea-level rise (Pieńkowski 2004; Haq 2017; Ruebsam et al. 2020; Bodin et al. 2023).

Stagnant conditions at the Pliensbachian–Toarcian boundary did not end at the beginning of the Tenuicostatum Zone, but continued through the whole zone (short-lived, slight improvement of oxygenation at the depth interval between 838.5 mbs and 847.0 mbs is too weak to be considered as significant break in the general stagnation). If the Tenuicostatum Zone was a cool period of time, then, according to the cooling/faster circulation paradigm, it would have resulted in a faster circulation throughout the entire zone. Instead, the Pliensbachian–Toarcian boundary event occurred at the beginning of long-lasting stagnation in Mochras. The sea-level rise postulated for this time interval (Pieńkowski 2004; Haq 2017; Ruebsam et al. 2020; Bodin et al. 2023) could have had some impact on deep-sea circulation, but it is uncertain in which direction. Sea-level rise would have led to lower energy of sedimentary processes and stagnation on continental shelves (due to the raised wave base), but it is unclear what would have happened in the case of much deeper water in the Cardigan Bay Basin. The influence of salinity drop in the early Toarcian epicontinental sea in UK (Remirez and Algeo 2020; Hesselbo et al. 2020b) could be considered as well, because density gradient is one of the main driving forces of deep-sea currents. By analogy with the recent Mediterranean and Atlantic waters (e.g., Bethoux et al. 1999), peri-Tethyan waters should have been more saline (due to evaporation) than waters in the Laurasian Seaway or Boreal Sea, where salinity could be diminished by freshwater influx from rivers and intermittent ice melt. However, the exact influence of the salinity gradient (which is elusive itself) on current intensity in the area studied remains uncertain.

The prolonged stagnation during the Tenuicostatum Zone could have resulted from coincidence of several overlapping causes, such as a warming phase of orbital forcing connected with a possible ~ 2.4 Myr grand eccentricity minimum, amplified by a concomitant warming effect, caused by initial Karoo volcanism emissions and consequent increase in pCO_2. Due to the mutual feedback effect and inertia of deep-sea oceanographic processes, this stagnation would last for a long time (~ 800 kyr). Stagnation of deep-sea circulation in the Laurasian seaway may challenge interpretations of continued cold conditions during the Tenuicostatum Zone, although the data from Yorkshire are unambiguous on this point (Korte et al. 2015, their Fig. 2). On the other hand, the Cleveland Basin could be a local anomaly, as some other reports (e.g., Ruebsam et al. 2020, their Fig. 5) claim that during the Tenuicostatum (= Polymorphum) Zone the Earth's climate system shifted between contrasting climatic conditions, particularly at the beginning and the end of this zone.

Extreme global warming occurred during the following Exaratum Subzone of the Serpentinum Zone, with benthic sea water temperature suggested to increase from ~ + 3 to 5 °C in mid-latitude Laurasian Seaway locations (see discussions in McArthur et al. 2000; Pálfy and Smith 2000; Gómez et al. 2008; Suan et al. 2010; Dera and Donnadieu 2012; Ullmann et al. 2020), or even as much as + 10 °C suggested for some sea-surface temperatures (Ruebsam et al. 2020). Such temperature increases, jointly with the demise of polar sea ice and stronger high-latitude continental runoff rates—which could have freshened the Arctic surface seawaters—would be expected to cause a general thermohaline circulation collapse (Dera and Donnadieu 2012). However, this is not evident in Mochras—instead, the Exaratum Subzone extreme global warming ended the previously dominating stagnation, counterarguing the previously supposed mechanism linking stagnation with warming. Likely, this time the global warming was so strong, that its consequences for deep-sea circulation were opposite—instead of sluggish circulation caused by northward currents only neutralizing dominating southward flow, the Tethyan northward flow became strong enough to prevail over the southward currents. As a consequence, the reversed deep-sea circulation became faster in the Cardigan Bay Basin. In particular, Dera and Donnadieu (2012) in their General Circulation Models (GCM) simulations found that for significantly higher pCO_2 levels (> 1600 ppm), the depth of mixed layer appears deeper in the European basins. This suggests a good ventilation of the water column during the To-CIE, which is obviously not the case in semi-closed, epicontinental seas in western Europe. However, since this simulation was based on a homogeneous epicontinental bathymetry of 200 m, even more significant results could be expected with a deeper bathymetry of the Cardigan Bay Basin. Moreover, it is worth noting that for other periods such as the Late Permian, GCM simulations show that massive rises in atmospheric CO_2 concentrations may drive more vigorous and more symmetrical deep-sea circulation under warmer climates (Winguth et al. 2002; Winguth and Maier-Reimer 2005).

According to Dera and Donnadieu (2012), the Exaratum Subzone thermal anomaly was probably related to a strengthening of warm equatorial Tethyan westward currents, drifting along the northern Gondwanan margins. Furthermore, the drift of these currents through westernmost areas and their subsequent clockwise rotation due to southward directed boreal flows is consistent with neodymium isotope data (Dera et al. 2009), as well as ammonite and nannofossil migration routes evidenced for the Early Toarcian (Reggiani et al. 2010; Dera et al.

2011). It is also likely that more vigorous NW Tethyan currents would account for major disruptions in faunal provincialism and northward expansion of marine Mediterranean faunas at the beginning of the Toarcian (Macchioni and Cecca 2002; Vörös 2002; Arias and Whatley 2005; Dera et al. 2011).

During the Tenuicostatum Zone to Exaratum Subzone period of time, the sedimentation rate in Mochras remained relatively stable and was still paced by precession (~ 20 kyr) and short- and long-eccentricity cycles (~ 100 and 405 kyr), which are all well expressed (Fig. 2a). Circulation decelerated just after the To-CIE event, in the earliest Falciferum Subzone (785–795 mbs), which is reflected by impoverished ichnodiversity and lithological features. From this time on, Toarcian circulation evidently became generally faster, particularly with regard to the middle parts of 1st order cycles, where more condensed sections and more frequent erosional/omission surfaces occur. The observations confirm that the warming/stagnation versus cooling/enhanced circulation mechanism returned after the To-CIE disturbances.

Importantly, existing data on sea-water temperature fluctuations in the Toarcian (McArthur et al. 2000; Gómez et al. 2008; Suan et al. 2010; Krencker et al. 2014; Ruebsam et al. 2020; Ullmann et al. 2020) support our conclusions regarding a large-scale correlation between sea-water temperature and inferred fluctuations of deep-sea current in the Cardigan Bay Basin. From the late Falciferum Subzone onwards, oxygenation of the sea floor generally improved; circulation intensity and average oxygenation achieved highest levels in the late Bifrons and Variabilis to earliest Thouarsense zones, as shown by sedimentological and ichnological features (Fig. 2b). This is likely associated with a long-term cooling trend, extending from the latest Falciferum Subzone to the Thouarsense Zone, with more intensified cooling in the Variabilis Zone. The latter was interrupted by a brief warming in the middle part of this zone (McArthur et al. 2000; Krencker et al. 2014). This brief warming seems to be also reflected in a slightly deteriorated ichnodiversity in Mochras (707–713 mbs), at the same time marking a boundary of ~ 2.4 Myr cycle.

The latest Thouarsense–Dispansum time interval in Mochras shows the next significant deterioration of ichnodiversity/oxygenation. This is likely connected to a warming trend that intensified in Dispansum Zone (Gómez et al. 2008), exactly when we are dealing with the conspicuous ichnodiversity/oxygenation crisis in Mochras. A weaker warming in the Pseudoradiosa Zone also corresponds to a slight deterioration of ichnodiversity around 610–615 mbs. The repetitive correlations between Toarcian sea-water temperature reconstructions elsewhere and contourite current intensity in the Cardigan Bay Basin point to a strong relationship between these variables, linking deep-sea circulation to major climate changes.

Toarcian sea-level changes are sometimes suspected as a possible factor in observed oceanographic processes. According to Ayranci et al. (2018), high-stand and transgressive-system tracts in Devonian contourites are represented by dominantly massive mudstone lithofacies, less intense bioturbation, and higher TOC values. Rising relative sea-level trends are confirmed for the Tenuicostatum Zone and also early Serpentinum, Bifrons and early Variabilis zones (Sellwood 1972; Graciansky et al. 1998; Pieńkowski 2004; Hesselbo 2008; Rocha et al. 2016; Barth et al. 2018; Haq 2017; Ruebsam and Al-Husseini 2021), but their relation to observed ichnological and sedimentological features in the Mochras profile is uncertain (Fig. 2a, b). Assuming a deep-sea setting of the Cardigan Bay Basin, major oceanographic/climate changes would have had a stronger impact than eustatic sea-level changes with amplitudes of only tens of metres (Haq 2017). Generally, a higher sea level might have enhanced the exchange of waters between adjacent basins and the circulation of currents, but the impact of eustatic (or tectonically-induced) sea level on deep-sea currents or the sediments entrained within them remains uncertain.

In addition to the beginning of the Toarcian (as discussed above), the relations between sedimentary (orbital) cycles and $\delta^{13}C$ fluctuations are not as clear as they were in older Early Jurassic stages at Mochras (Storm et al. 2020). Some of the minor negative excursions at depths of 750, 719, 697, 675, 667 and 630 mbs seem to be related with more stagnant conditions (short-lived minor *Phycosiphon* crises, appearances of lamination and *Trichichnus*), but this relation requires more systematic study and a much higher resolution C-isotope curve. This is particularly important in the upper part of the profile, where the variations in $\delta^{13}C$ values are subdued.

4.4 Duration of the Toarcian and ammonite zones based on ichnological astrochronology

The Toarcian section of the Mochras core represents the most expanded and highest resolution cyclostratigraphic dataset for this stage to date (even if much of the Aalensis Zone is eroded), and provides the most reliable basis for an astrochronological time scale, reflecting Milankovitch forcing, predominantly at precession/obliquity and the short- and long-eccentricity periodicities (Fig. 2a, b). The new results allow an estimation of the duration of the Toarcian stage at a minimum of 9.4 Myr (without most of the Aalensis Zone). Results were obtained from ichnological and sedimentological signals by counting successive 4th, 3rd and 2nd order cycles (interpreted respectively as

Table 3 Duration of Toarcian biochronozones

Aalensis	> 0.1 Myr
Pseudoradiosa	1.4 ± 0.02 Myr
Dispansum	0.3 ± 0.07 Myr
Thouarsense	0.8 ± 0.1 Myr
Variabilis	2.4 ± 0.1 Myr
Bifrons	2.1 ± 0.5 Myr
Serpentinum	1.4 ± 0.4 Myr
Tenuicostatum	0.9 ± 0.1 Myr
TOARCIAN	> 9.4 Myr

Note that most of the *Aalensis* Zone is missing in the Mochras section. All durations are minima and the uncertainties relate only to precision of the placement of the zonal boundaries in the core based on ammonite distributions recorded in Additional files 3–5

precession/obliquity, short eccentricity, long eccentricity). Uncertainty values of zone durations are estimated based on depth-domain uncertainties of zonal boundaries (Additional file 3). For each zone, summed uncertainties of the base and top boundary are treated as a percentage of nominal zone thickness and proportionally converted to time domain. In case of the Dispansum and Pseudoradiosa zones the time-domain uncertainties are represented by spurious digits and are therefore negligible. Astronomical durations for the ammonite chronozones (based mainly on ~ 405 kyr, 2nd order cycles) are: Tenuicostatum Zone = 0.9 ± 0.1 Myr, Serpentinum Zone = 1.4 ± 0.4 Myr, Bifrons Zone = 2.1 ± 0.5 Myr, Variabilis Zone = 2.4 ± 0.1 Myr, Thouarsense Zone = 0.8 ± 0.1 Myr, Dispansum Zone = 0.3 ± 0.07 Myr, Pseudoradiosa Zone = 1.4 ± 0.02 Myr. The Aalensis Zone (truncated at its top) is preserved probably representing no more than 0.5 Myr of deposition. The obtained durations of successive ammonite zones (Table 3) are slightly longer compared to those shown in GTS2020 (Hesselbo et al. 2020a).

5 Conclusions

1. An integrated ichnological-sedimentological study of the Toarcian siliciclastic-calcareous contourite deposits in Mochras helps facilitate understanding of contourite deposition processes over a long period of geological time and its ichnodiversity. Together with the Pliensbachian part of the section (Pieńkowski et al. 2021), the current study comprises an expanded ichnological and sedimentary record of contourite deposits, adding new information on the sedimentary dynamics, variability of oceanographic history, and basin interconnectivity.
2. Ichnological signals point to a common and strongly repetitive mechanism driving the observed fluctuations in benthic conditions, which is indicated by spectral analysis and distinction of four hierarchical orders of cycles attributed to orbital forcing.
3. Long-term climate change controlled the circulation of contour-parallel bottom currents in the Cardigan Bay Basin and orbital forcing has set the timing for cyclic ichnological records, with the amplifying feedback of climate-related palaeoceanographic variations of thermohaline-driven contour currents circulating between the Boreal ocean and Peri-Tethys, through the Cardigan Bay Strait. There is continuity of ~ 2.4 Myr, rather than ~ 1.6 Myr cyclicity expressed in deep-sea circulation and the probable occurrence of yet longer, ~ 7–8 Myr (~ 7.5) periodicity which may or may not be under an orbital control. The mutual modulation of the two cyclicities (~ 3.4 and ~ 1.6 Myr) indicated by Charbonier et al. (2023), giving approximately the resultant cyclicity of 2.4–2.5 Myr observed in Mochras would be a plausible explanation, if the hypothesis of chaotic behaviour of the Solar System in Mesozoic is confirmed.
4. In more temperate climates, the formation of high-density waters was associated with low temperatures at higher latitudes and sinking of cooler and denser water masses, which then flowed south. However, in the early Toarcian this secular, extrinsic paradigm has been modified due to intrinsic Earth processes related to large-scale volcanism and higher temperatures, which led to intense evaporation and increase in salinity in the middle latitudes. This hypothetically began to play a dominant role in circulation, stopping or reversing the directions of marine currents, which resulted in a temporal disturbance of a long-term orbitally-controlled mechanism, but without eliminating the influence of orbital forcing.
5. The most severe oxygen crisis (dysoxic, but not anoxic), evidenced by trace fossils (*Phycosiphon* scarcity, mass appearances of *Trichichnus*) commenced shortly before the Pliensbachian-Toarcian boundary and ended at the early stage of the Toarcian negative carbon isotope excursion (To-CIE), which is in contrast to the general pattern of the T-OAE anoxic phenomenon in relatively shallow marine settings and its synchroneity with the To-CIE. The extreme climate warming, coeval to To-CIE, is therefore hypothesised to have caused significant changes in deep marine circulation, reversing its direction and improving oxygenation of the deep-sea floor.
6. Ichnological results, both macroscopic observations and spectral analysis, confirm the cycles that appear in the Mochras visual descriptions, and a new minimum estimate of duration of the Toarcian (9.4 Myr) and constituent ammonite zones is proposed.

7. Contourites of the Cardigan Bay Basin provide information on inter-ocean circulation, benthic conditions, and climate changes, which can be extracted using sedimentological and ichnological methods. The Cardigan Bay Strait played an important role in the Early Jurassic (at least Pliensbachian and Toarcian) marine circulation as a major link between the northern and southern part of the Laurasian Seaway, and in general between the Boreal and peri-Tethys oceanic domains.
8. Ichnological records in continuous hemipelagic successions seem to be a sensitive and reliable basis for the recognition of cyclic orbital forcing of climatic and palaeoceanographic conditions. Smoothed curves based on specific ichnotaxa occurrence time series bear resemblance to geochemical and geophysical proxy records, indicating concurrent response to the changing environmental conditions.

Abbreviations

To-CIE Toarcian negative carbon isotope excursion
T-OAE Toarcian oceanic anoxic event

Supplementary Information

The online version contains supplementary material available at https://doi.org/10.1186/s40645-024-00612-3.

Additional file 1. Matrix of binary time series used for spectral analysis.

Additional file 2. Description of time series and the runs test methodology and results.

Additional file 3. Toarcian ammonite biozones for the Llanbedr (Mochras Farm) borehole, compiled from KN Page in Copestake and Johnson (2014) and McArthur et al. (2016); refer to Additional files 4 and 5 for details.

Additional file 4. Biostratigraphically significant ammonite fossils from the Lower Toarcian of the Llanbedr (Mochras Farm) borehole, Wales, and proposed correlations to Yorkshire coast outcrops; all fossil identifications by KN Page.

Additional file 5. Biostratigraphically significant ammonite fossils from the Upper Toarcian of the Llanbedr (Mochras Farm) borehole, Wales; all fossil identifications by KN Page.

Acknowledgements

The National Geological Repository of the British Geological Survey, Keyworth, Nottingham, UK, is acknowledged for sharing the Mochras drill core for investigations. There staff are warmly thanked for longstanding support of this project. Two anonymous reviewers provided corrections and helpul comments.

Author contributions

GP: conceptualization, data curation, formal analysis, investigation, writing—original draft (lead); AU: conceptualization, data curation, formal analysis, investigation, funding acquisition (lead), project administration (lead from the National Science Centre, Poland side), writing—review and editing; KN: numerical analyses (lead), writing—review and editing (partial); KNP: refinement of ammonite biostratigraphy; SPH: conceptualization, review and editing, funding acquisition (partial), formal analysis, project administration (lead from the ICDP and NERC project JET sides).

Funding

The research is financed by the National Science Centre, Poland, from the programme Opus 13, Grant Agreement No. 2017/25/B/ST10/02235 and the internal Polish Geological Institute Grant No. 62.9012.2016.00.0. This is a contribution to the ICDP and NERC JET Project: SPH and KNP were supported from the Natural Environment Research Council (NERC), Grant No. NE/N018508/1. For the purpose of open access, the author has applied a 'Creative Commons Attribution (CC BY) licence to any Author Accepted Manuscript version arising from this submission.

Availability of data and materials

All data generated during this study are included in the paper and its Additional files. Downhole log data from Mochras are available via the UK Onshore Geophysical Library (UKOGL) website https://ukogl.org.uk/.

Declarations

Competing interests

The authors declare that they have no known competing financial interests or personal relationships that could have appeared to influence the work reported in this paper.

Author details

[1]Polish Geological Institute–National Research Institute, Rakowiecka 4, 00-975 Warsaw, Poland. [2]Faculty of Geography and Geology, Jagiellonian University, Gronostajowa 3a, 30-087 Kraków, Poland. [3]Department of Earth and Environmental Sciences, University of Exeter, Penryn Campus, Cornwall TR10 9FE, UK.

Received: 16 June 2023 Accepted: 17 February 2024
Published online: 29 March 2024

References

Alpert SP (1974) Systematic review of the genus *Skolithos*. J Paleont 49:509–521

Al-Suwaidi AH, Ruhl M, Jenkyns HC, Damborenea SE, Manceñido MO, Condon DJ, Angelozzi GN, Kamo SL, Storm M, Riccardi AC, Hesselbo SP (2022) New age constraints on the Lower Jurassic Pliensbachian-Toarcian Boundary at Chacay Melehue (Neuquén Basin, Argentina). Sci Rep 12(1):4975. https://doi.org/10.1038/s41598-022-07886-x

Arias C, Whatley RC (2005) Palaeozoogeography of Western European Lower Jurassic (Pliensbachian and Toarcian) Ostracoda. Geobios 38:697–724. https://doi.org/10.1016/j.geobios.2002.10.001

Ausich WI, Bottjer DJ (1982) Tiering in suspension-feeding communities on soft substrata throughout the Phanerozoic. Science 216:173–174. https://doi.org/10.1126/science.216.4542.173

Atkinson JW, Little CTS, Dunhill AM (2022) Long duration of benthic ecological recovery from the early Toarcian (Lower Jurassic) mass extinction event in the Cleveland Basin. UK J Geol Soc. https://doi.org/10.1144/jgs2022-126

Ayranci K, Harris NB, Dong T (2018) High resolution sequence stratigraphic reconstruction of mud-dominated systems below storm wave base; a case study from the Middle to Upper Devonian Horn River Group, British Columbia, Canada. Sediment Geol 373:239–253. https://doi.org/10.1016/j.sedgeo.2018.06.009

Baldwin CT, McCave IN (1999) Bioturbation in an active deep-sea area: implications for models of trace fossil tiering. Palaios 14:375–388. https://doi.org/10.2307/3515463

Baucon A, Bednarz M, Dufour S, Felletti F, Malgesini G, Neto de Carvalho C, Niklas KJ, Wehrmann A, Batstone R, Bernardini F, Briguglio A, Cabella R, Cavalazzi B, Ferretti A, Zanzerl H, McIlroy D (2020) Ethology of the trace fossil *Chondrites*: form, function and environment. Earth-Sci Rev 202:102989. https://doi.org/10.1016/j.earscirev.2019.102989

Barth G, Pieńkowski G, Zimmermann J, Franz M, Kuhlmann G (2018) Palaeogeographical evolution of the Lower Jurassic: high-resolution biostratigraphy and sequence stratigraphy in the Central European Basin. In: Kilhams B, Kukla PA, Mazur S, McKie T, Mijnlieff HF, Van Ojik K (eds) Mesozoic resource potential in the Southern Permian Basin. Geological Soc London Spec Publ, vol 469, pp 341–369. https://doi.org/10.1144/SP469.8

Bednarz M, McIlroy D (2009) Three-dimensional reconstruction of "phycosiphoniform" burrows: implications for identification of trace fossils in core. Palaeont Electron 12(3):13A

Bein A, Weiler Y (1976) The Cretaceous Talme Yafe Formation: a contour current shaped sedimentary prism of calcareous detritus at the continental margin of the Arabian craton. Sedimentology 23:511–532. https://doi.org/10.1111/j.1365-3091.1976.tb00065.x

Berger AL (1977) Support for the astronomical theory of climatic change. Nature 269:44–45. https://doi.org/10.1038/269044a0

Bethoux JP, Gentili B, Morin P, Nicolas E, Pierre C, Ruiz-Pino D (1999) The Mediterranean Sea: a miniature ocean for climatic and environmental studies and a key for the climatic functioning of the North Atlantic. Progr Oceanogr 44:131–146. https://doi.org/10.1016/S0079-6611(99)00023-3

Bjerrum CJ, Surlyk F, Callomon JH, Slingerland RL (2001) Numerical paleoceanographic study of the Early Jurassic Transcontinental Laurasian seaway. Paleoceanography 16:390–404. https://doi.org/10.1029/2000PA000512

Bodin S, Krencker FN, Kothe T, Hoffmann R, Mattioli E, Heimhofer U, Kabiri L (2016) Perturbation of the carbon cycle during the late Pliensbachian–early Toarcian: New insight from high-resolution carbon isotope records in Morocco. J Afr Earth Sci 116:89–104. https://doi.org/10.1016/j.jafrearsci.2015.12.018

Bodin S, Fantasia A, Krencker F-N, Nebsbjerg B, Christiansen L, Andrieuet S (2023) More gaps than record! A new look at the Pliensbachian/Toarcian boundary event guided by coupled chemo-sequence stratigraphy. Palaeogeogr Palaeoclimat Palaeoecol 610:111344. https://doi.org/10.1016/j.palaeo.2022.111344

Boomer ID (1991) Lower Jurassic ostracod biozonation of the Mochras borehole. J Micropalaeont 9:205–218. https://doi.org/10.1144/jm.9.2.205

Boulila S, Hinnov LA (2017) A review of tempo and scale of the early Jurassic Toarcian OAE: implications for carbon cycle and sea level variations. Newslett Stratigr 50(4):363–389. https://doi.org/10.1127/nos/2017/0374

Boulila S, Galbrun B, Huret E, Hinnov LA, Rouget I, Gardin S et al (2014) Astronomical calibration of the Toarcian Stage: implications for sequence stratigraphy and duration of the early Toarcian OAE. Earth Planet Sci Lett 386:98111. https://doi.org/10.1016/j.epsl.2013.10.047

Boulila S, Galbrun B, Sadki D, Gardin S, Bartolini A (2019) Constraints on the duration of the early Toarcian T-OAE and evidence for carbon-reservoir change from the High Atlas (Morocco). Glob Planet Change 175:113128. https://doi.org/10.1016/j.earscirev.2011.09.003

Boulila S, Vahlenkamp M, De Vleeschouwer D, Laskar J, Yamamoto Y, Pälike H, Kirtland Turner S, Sexton PF, Westerhold T, Röhl U (2018) Towards a robust and consistent middle Eocene astronomical timescale. Earth Planet Sci Lett 486:94–107. https://doi.org/10.1016/j.epsl.2018.01.003

Bouma AH (1962) Sedimentology of some flysch deposits. Elsevier, Amsterdam

Bown PR (1987) Taxonomy, evolution and biostratigraphy of Late Triassic-Early Jurassic calcareous nannofossils. Special papers in paleontology, vol 38. The Palaeontological Association, London

Brandt K (1986) Glacioeustatic cycles in the Early Jurassic? Neues Jb Geol Paläont Mh 5:257–274. https://doi.org/10.1127/njgpm/1986/1986/257

Bromley RG (1991) *Zoophycos*: strip mine, refuse dump, cache or sewage farm? Lethaia 24:460–462. https://doi.org/10.1111/j.1502-3931.1991.tb01501.x

Bromley RG (1996) Trace fossils. Biology, taphonomy and applications, 2nd edn. Chapman & Hall, London

Bromley RG, Uchman A (2003) Trace fossils from the Lower and Middle Jurassic marginal marine deposits of the Sorthat Formation, Bornholm, Denmark. Bull Geol Soc 52:185–208

Callow RHT, McIlroy D, Kneller B, Dykstra M (2013) Integrated ichnological and sedimentological analysis of a Late Cretaceous submarine channel-levee system: the Rosario Formation, Baja California, Mexico. Mar Petrol Geol 41:277–294. https://doi.org/10.1016/j.marpetgeo.2012.02.001

Caswell BA, Frid CLJ (2017) Marine ecosystem resilience during extreme deoxygenation: the Early Jurassic oceanic anoxic event. Oecologia 183:275–290. https://doi.org/10.1007/s00442-016-3747-6

Charbonnier G, Boulila S, Galbrun B, Laskar J, Garden S, Rouget I (2023) A 20-million-year Early Jurassic cyclostratigraphic record and its implications for the chaotic inner Solar System and sea-level changes. Basin Res. https://doi.org/10.1111/bre.12754

Cope JCW, Ingham JK, Rawson PF (eds) (1992) Atlas of palaeogeography and lithofacies. Geological Society, London

Copestake P, Johnson B (2014) Lower Jurassic foraminifera from the Llanbedr (Mochras Farm) borehole, North/Wales, UK. Monog Palaeontogr Soc Lond 167:1–403. https://doi.org/10.1080/02693445.2013.11963952

Crimes TP (1977) Trace fossils of an Eocene deep-sea fan, northern Spain. In: Crimes TP, Harper JC (eds) Trace fossils 2. Geol Jour Spec Iss, vol 9, pp 71–90

Dashtgard SE (2011) Neoichnology of the lower delta plain: Fraser River Delta, British Columbia, Canada: implications for the ichnology of deltas. Palaeogeogr Palaeoclimat Palaeoecol 307:98–108. https://doi.org/10.1016/j.palaeo.2011.05.001

De Boor C (2001) A practical guide to splines, Revised. Springer, New York

Deconinck JF, Hesselbo SP, Pellenard P (2019) Climatic and sea-level control of Jurassic (Pliensbachian) clay mineral sedimentation in the Cardigan Bay Basin, Llanbedr (Mochras Farm) borehole Wales. Sedimentology 66:2769–2783. https://doi.org/10.1111/sed.12610

Dera G, Pucéat E, Pellenard P, Neige P, Delsate D, Joachimski MM, Reisberg L, Martinez M (2009) Water mass exchange and variations in seawater temperature in the NW Tethys during the Early Jurassic: evidence from neodymium and oxygen isotopes of fish teeth and belemnites. Earth Planet Sci Lett 286:198–207. https://doi.org/10.1016/j.epsl.2009.06.027

Dera G, Donnadieu Y (2012) Modeling evidences for global warming, Arctic seawater freshening, and sluggish oceanic circulation during the Early Toarcian anoxic event. Paleoceanography 27:PA2211. https://doi.org/10.1029/2012PA002283

Dera G, Neige P, Dommergues J-L, Brayard A (2011) Ammonite paleobiogeography during the Pliensbachian–Toarcian crisis (Early Jurassic) reflecting paleoclimate, eustasy, and extinctions. Glob Planet Change 78:92–105. https://doi.org/10.1016/j.gloplacha.2011.05.009

Dobson MR, Whittington RJ (1987) The geology of Cardigan Bay. Proc Geol Assoc 98:331–353. https://doi.org/10.1016/S0016-7878(87)80074-3

Dorador J, Rodríguez-Tovar FJ, Mena A, Francés G (2019) Lateral variability of ichnological content in muddy contourites: weak bottom currents affecting organisms' behavior. Sci Rep 9:17713. https://doi.org/10.1038/s41598-019-54246-3

Dunham RJ (1962) Classification of carbonate rocks according to depositional texture. In: Ham, WE (ed) Classification of carbonate rocks. AAPG Memoir, vol 1, pp 108–121

Ekdale AA (1985) Paleoecology of the marine endobenthos. Palaeogeogr Palaeoclimat Palaeoecol 50:63–81. https://doi.org/10.1016/S0031-0182(85)80006-7

Ekdale AA (1992) Muckraking and mudslinging: the joys of deposit-feeding. In: Maples CG, West RR (eds) Trace fossils. Short Cours Paleont, vol 5. The Paleontological Society, Knoxville, pp 145–171

Ekdale AA, Lewis DW (1991) The New Zealand *Zoophycos* revisited. Ichnos 1:183–194. https://doi.org/10.1080/10420949109386351

Erba E, Premoli Silva I (1994) Orbitally driven cycles in trace-fossil distribution from the Piobicco core (late Albian, central Italy). Spec Publ Inst Ass Sediment 19:211–225. https://doi.org/10.1002/9781444304039.ch16

Esmerode EV, Lykke-Andersen HF, Surlyk F (2008) Interaction between bottom currents and slope failure in the Late Cretaceous of the southern Danish Central Graben, North Sea. J Geol Soc Lond 165:55–72. https://doi.org/10.1144/0016-76492006-138

Ewing M, Thorndike EM (1965) Suspended matter in deep ocean waters. Science 147:1291–1294. https://doi.org/10.1126/science.147.3663.1291

Fantasia A, Föllmi KB, Adatte T, Spangenberg JE, Montero-Serrano JC (2018) The Early Toarcian oceanic anoxic event: Paleoenvironmental and paleoclimatic change across the Alpine Tethys (Switzerland). Glob Planet Change 162:53–68. https://doi.org/10.1016/j.gloplacha.2018.01.008

Farrow GE (1966) Bathymetric zonation of Jurassic trace fossils from the coast Yorkshire, England. Palaeogeogr Palaeoclimat Palaeoecol 2:103–151. https://doi.org/10.1016/0031-0182(66)90011-3

Faugeres J-C, Gonthier E, Stow DAV (1984) Contourite drift moulded by deep Mediterranean outflow. Geology 12:296–300. https://doi.org/10.1130/0091-7613(1984)12%3c296:CDMBDM%3e2.0.CO;2
Faugeres JC, Mulder T (2011) Contour currents and contourite drifts. In: Huneke H, Mulder T (eds) Deep-sea sediments. Developments in Sedimentology, vol 63. Elsevier, Amsterdam, pp 149–214. https://doi.org/10.1016/B978-0-444-53000-4.00003-2
Faugères J-C, Stow DAV (2008) Contourite drifts: nature, evolution and controls. In: Rebesco M, Camerlenghi A (eds) Contourites. Developments in sedimentology, vol 60. Elsevier, Amsterdam, pp 257–288. https://doi.org/10.1016/S0070-4571(08)10014-0
Fillion D, Pickerill RK (1990) Ichnology of the Upper Cambrian? to Lower Ordovician Bell Island and Wabana groups of eastern Newfoundland, Canada. Palaeontogr Canad 7:1–119
Fischer-Ooster C (1858) Die fossilen Fucoiden der Schweizer-Alpen, nebst Erörterungen über deren geologisches. Alter. Huber, Bern
Frey RW (1970) Trace fossils of Fort Hays Limestone Member of Niobrara Chalk (Upper Cretaceous) West-Central Kansas. Univ Kansas Paleont Contrib 53:1–41
Frey RW, Bromley RG (1985) Ichnology of American chalks: the Seelma Group (Upper Cretaceous), western Alabama. Can J Earth Sci 22:801–822. https://doi.org/10.1139/e85-087
Frey RW, Curran AH, Pemberton GS (1984) Trace making activities of crabs and their environmental significance: the ichnogenus *Psilonichnus*. J Paleont 58:333–350
Frey RW, Goldring R (1992) Marine event beds and recolonization surfaces as revealed by trace fossil analysis. Geol Mag 129:325–335. https://doi.org/10.1017/S0016756800019269
Frey RW, Howard JD, Pryor WA (1978) *Ophiomorpha*: its morphologic, taxonomic, and environmental significance. Palaeogeogr Palaeoclimat Palaeoecol 23:199–223
Fu S (1991) Funktion, Verhalten und Einteilung fucoider und lophocteniider Lebensspuren. Courier Forsch Senckenberg 135:1–79. https://doi.org/10.1016/0031-0182(78)90094-9
Fürsich FT (1973) A revision of the trace fossils *Spongeliomorpha*, *Ophiomorpha* and *Thalassinoides*. N Jb Geol Pal Mh 12:719–735
Fürsich FT (1974) Ichnogenus *Rhizocorallium*. Paläont Zeitschr 48:16–28. https://doi.org/10.1007/BF02986987
Fürsich FT, Mayr H (1981) Non-marine Rhizocorallium (trace fossil) from the Upper Freshwater Molasse (upper Miocene) of southern Germany. Neues Jb Geol Paläont Mh 6:321–333. https://doi.org/10.1127/njgpm/1981/1981/321
Gingras MK, Dashtgard SE, MacEachern JA, Pemberton SG (2008) Biology of shallow-marine ichnology: a modern perspective. Aquat Biol 2:255–268. https://doi.org/10.3354/ab00055
Goldring R (1962) Trace fossils of the Baggy Beds (Upper Devonian) of North Devon, England. Paläont Zeitschr 36:232–251
Goldring R, Pollard JE, Taylor AM (1991) *Anconichnus horizontalis*: a pervasive ichnofabric-forming trace fossil in the Post-Paleozoic offshore siliciclastic facies. Palaios 6:250–263. https://doi.org/10.2307/3514905
Gómez JJ, Goy A, Canales ML (2008) Seawater temperature and carbon isotope variations in belemnites linked to mass extinction during the Toarcian (Early Jurassic) in Central and Northern Spain. Comparison with other European sections. Palaeogeogr Palaeoclim Palaeoecol 258:28–58. https://doi.org/10.1016/j.palaeo.2007.11.005
Gong C, Peakall J, Wang Y, Wells MG, Xu J (2017) Flow processes and sedimentation in contourite channels on the northwestern South China Sea margin: a joint 3D seismic and oceanographic perspective. Mar Geol 393:176–193. https://doi.org/10.1016/j.margeo.2016.11.002
Graciansky PC, de Jacquin T, Hesselbo PS (1998) The Ligurian cycle: an overview of Lower Jurassic 2nd-order transgressive/regressive facies cycles in Western Europe. In: Graciansky PC, de Hardenbol J, Jacquin T, Vail PR (eds) Mesozoic and Cenozoic Sequence Stratigraphy of European Basins. Soc Econ Paleont Miner Spec Publ 60:467–479. https://doi.org/10.2110/pec.98.02.0467
Guex J, Morard A, Bartolini A, Morettini E (2001) Discovery of an important stratigraphic gap at the Domerian-Toarcian limit: Palaeo-oceanographic implications. Bull Soc Vaudoise Sci Nat 87:277–284
Hakes WG (1976) Trace fossils and depositional environment of four clastic units, Upper Pennsylvanian megacyclothems, northeast Kansas. Univ Kansas Palaeont Contrib 63:1–46
Hallam A, Swett K (1966) Trace fossils from the Lower Cambrian Pipe Rock of the north-west Highlands. Scott J Geol 2:101–106
Hammer Ø, Harper DAT, Ryan PD (2001) PAST: paleontological statistics software package for education and data analysis. Palaeont Electr 4(1):9 pp. http://palaeo-electronica.org/2001_1/past/issue1_01.htm
Hammer Ø, Harper DAT (2006) Paleontological data analysis. Blackwell, Oxford
Haq BU (2017) Jurassic sea-level variations: a reappraisal. GSA Today 28:4–10. https://doi.org/10.1130/GSATG359A.1
Hermoso M, Le Callonnec L, Minoletti F, Renard M, Hesselbo SP (2009) Expression of the Early Toarcian negative carbon-isotope excursion in separated carbonate microfractions (Jurassic, Paris Basin). Earth Planet Sci Lett 277:194–203. https://doi.org/10.1016/j.epsl.2008.10.013
Hesselbo SP (2008) Sequence stratigraphy and inferred relative sea-level change from the onshore British Jurassic. Proc Geol Assoc 119:19–34. https://doi.org/10.5194/sd-16-81-2013
Hesselbo SP, Pieńkowski G (2011) Stepwise atmospheric carbon-isotope excursion during the Toarcian oceanic anoxic event (Early Jurassic, Polish Basin). Earth Planet Sci Lett 301:365–372. https://doi.org/10.1016/j.epsl.2010.11.021
Hesselbo SP, Gröcke DR, Jenkyns HC, Bjerrum CJ, Farrimond P, Morgans Bell HS, Green OR (2000) Massive dissociation of gas hydrate during a Jurassic oceanic anoxic event. Nature 406:392–395. https://doi.org/10.1038/35019044
Hesselbo SP, Jenkyns HC, Duarte LV, Oliveira LC (2007) Carbon-isotope record of the Early Jurassic (Toarcian) Oceanic Anoxic Event from fossil wood and marine carbonate (Lusitanian Basin, Portugal). Earth Planet Sci Lett 253:455–470. https://doi.org/10.1016/j.epsl.2006.11.009
Hesselbo SP, Bjerrum CJ, Hinnov LA, MacNiocaill C, Miller KG, Riding JB, Van de Schootbrugge B, the Mochras Revisited Science Team (2013) Mochras borehole revisited: a new global standard for Early Jurassic Earth history. Sci Drill 16:81–91. https://doi.org/10.5194/sd-16-81-2013
Hesselbo SP, King C (2019) Stratigraphic Framework for the Yorkshire Lias. In: Lord A (ed) Fossils of the Lias of Yorkshire. Palaeontological Association, London, pp 30–40
Hesselbo SP, Ogg JG, Ruhl M (2020a) The Jurassic period. In: Gradstein FM, Ogg JG, Schmitz MD, Ogg GM (eds) Geologic Time Scale 2020. Elsevier, Hoboken, pp 955–1021
Hesselbo SP, Little CTS, Ruhl M, Thibault N, Ullmann CV (2020b) Comments on "Paleosalinity determination in ancient epicontinental seas: a case study of the TOAE in the Cleveland Basin (UK)" by Remirez, M. N. and Algeo, T. J. Earth Sci Rev. https://doi.org/10.1016/j.earscirev.2020.103290
Hesselbo SP et al (2023) Initial results of coring at Prees, Cheshire Basin, UK (ICDP JET Project); towards an integrated stratigraphy, timescale, and Earth system understanding for the Early Jurassic. Sci Drill 32:1–25. https://doi.org/10.5194/sd-32-1-2023
Hinnov LA (2000) New perspectives on orbitally forced stratigraphy. Annu Rev Earth Planet Sci 28:419–475. https://doi.org/10.1146/annurev.earth.28.1.419
Hollaar TP, Hesselbo SP, Deconinck J-F, Damaschke M, Ullmann CV, Jiang M, Belcher CM (2023) Environmental changes during the onset of the Late Pliensbachian Event (Early Jurassic) in the Cardigan Bay Basin, Wales. Clim past 19:979–997. https://doi.org/10.5194/cp-2022-87
Huang C (2018) Astronomical time scale for the Mesozoic. Stratigraphy and time scales, vol 3. Elsevier, Hoboken, pp 81–150. https://doi.org/10.1016/bs.sats.2018.08.005
Huang C, Hesselbo SP (2014) Pacing of the Toarcian Oceanic Anoxic Event (Early Jurassic) from astronomical correlation of marine sections. Gondwana Res 25:1348–1356. https://doi.org/10.1016/j.gr.2013.06.023
Huang H, Gao Y, Ma C, Jones MM, Zeeden C, Ibarra DE, Wu H, Wang C (2021) Organic carbon burial is paced by a ~173-ka obliquity cycle in the middle to high latitudes. Sci Adv 7:eabf9489. https://doi.org/10.1126/sciadv.abf9489
Huret E, Hinnov LA, Galbrun B, Collin P-Y, Gardin S, Rouget I (2008) Astronomical calibration and correlation of the Lower Jurassic, Paris and Lombard basins (Tethys). 33rd International Geological Congress, Oslo, Norway, Abstract
Hüneke NV, Stow DAV (2008) Identification of ancient contourites: problems and palaeoceanographic significance. In: Rebesco M, Camerlenghi A (eds) Contourites. Developments in sedimentology, vol 60. Elsevier, Amsterdam, pp 323–344. https://doi.org/10.1016/S0070-4571(08)10017-6

Ikeda M, Tada R (2013) Long period astronomical cycles from the Triassic to Jurassic bedded chert sequence (Inuyama, Japan); geologic evidences for the chaotic behavior of solar planets. Earth Planets Space 65:351–360. https://doi.org/10.5047/eps.2012.09.004
Ikeda M, Tada R (2020) Reconstruction of the chaotic behavior of the Solar System from geologic records. Earth Planet Sci Lett 537:116168. https://doi.org/10.1016/j.epsl.2020.116168
Ikeda M, Hori RS, Ikehara M, Miyashita R, Chino M, Yamada K (2018) Carbon cycle dynamics linked with Karoo-Ferrar volcanism and astronomical cycles during Pliensbachian-Toarcian (Early Jurassic). Glob Planet Change 170:163–171. https://doi.org/10.1016/j.gloplacha.2018.08.012
Izumi K (2014) Utility of geochemical analysis of trace fossils: case studies using Phycosiphon incertum from the Lower Jurassic shallow-marine (Higashinagano Formation, southwest Japan) and Pliocene deep-marine deposits (Shiramazu Formation, central Japan). Ichnos 21:62–72. https://doi.org/10.1080/10420940.2013.877008
Jenkyns HC, Jones CE, Gröcke DR, Hesselbo SP, Parkinson DN (2002) Chemostratigraphy of the Jurassic System: applications, limitations and implications for palaeoceanography. J Geol Soc Lond 159:351–378. https://doi.org/10.1144/0016-764901-13
Jensen S (1997) Trace fossils from the Lower Cambrian Mickwitzia Sandstone, south-central Sweden. Fossils Strata 42:1–110
Kędzierski M, Uchman A, Sawłowicz Z, Briguglio A (2015) Fossilized bioelectric wire: the trace fossil *Trichichnus*. Biogeosciences 12:2301–2309. https://doi.org/10.5194/bg-12-2301-2015
Kemp DB, Coe AL, Cohen AS, Schwark L (2005) Astronomical pacing of methane release in the Early Jurassic period. Nature 437:396–399. https://doi.org/10.1038/nature04037
Kemp DB, Coe AL, Cohen AS, Weedon GP (2011) Astronomical forcing and chronology of the early Toarcian (Early Jurassic) Oceanic Anoxic Event in Yorkshire, UK. Paleoceanography 26:PA4210. https://doi.org/10.1029/2011PA002122
Kemp DB, Fraser WT, Izumi K (2018) Stratigraphic completeness and resolution in an ancient mudrock succession. Sedimentology 65:1875–1890. https://doi.org/10.1111/sed.12450
Kennedy WJ (1975) Trace fossils in carbonate rocks. In: Frey RW (ed) The study of trace fossils. Springer, New York, pp 377–398
Kent DV, Olsen PE, Rasmussen C, Lepre C, Mundil R, Irmis RB, Gehrels GE, Giesler D, Geissman JW, Parker WG (2018) Empirical evidence for stability of the 405-kiloyear Jupiter-Venus eccentricity cycle over hundreds of millions of years. Proc Natl Acad Sci USA 115:6153–6158. https://doi.org/10.1073/pnas.1800891115
Kjeldsen KU, Schreiber L, Thorup CA, Boesen T, Bjerg JT, Yang T, Dueholm MS, Larsen S, Risgaard-Petersen N, Nierychlo M, Schmid M, Bøggild A, Vossenberg J, van de Geelhoedi JS, Meysman FJR, Wagner M, Nielsen PH, Nielsena LP, Schramm A (2019) On the evolution and physiology of cable bacteria. Proc Natl Acad Sci USA 116:19116–19125. https://doi.org/10.1073/pnas.1903514116
Knapp LJ, McMillan JM, Harris NB (2017) A depositional model for organic-rich Duvernay Formation mudstones. Sediment Geol 347:160–182. https://doi.org/10.1016/j.sedgeo.2016.11.012
Knaust D (2013) The ichnogenus *Rhizocorallium*: classification, trace makers, palaeoenvironments and evolution. Earth Sci Rev 126:1–47. https://doi.org/10.1016/j.earscirev.2013.04.007
Knaust D (2015) Siphonichnidae (new ichnofamily) attributed to the burrowing activity of bivalves: ichnotaxonomy, behaviour and palaeoenvironmental implications. Earth Sci Rev 150:497–519. https://doi.org/10.1016/j.earscirev.2015.07.014
Knaust D (2017) Atlas of trace fossils in well core: appearance, taxonomy and interpretation. Springer, Berlin, p 271
Knaust D, Warchoł M, Kane IA (2014) Ichnodiversity and ichnoabundance: revealing depositional trends in a confined turbidite system. Sedimentology 61:2218–2267. https://doi.org/10.1111/sed.12134
Koopmans MP, Köster J, van Kaam-Peters HME, Kenig F, Schouten S, Hartgers WA, de Leeuw JW, Sinninghe Damsté JS (1996) Diagenetic and catagenetic products of isorenieratane: molecular indicators for photic zone anoxia. Geochim Cosmochim Acta 60:4467–4496. https://doi.org/10.1016/S0016-7037(96)00238-4
Korte C, Hesselbo SP (2011) Shallow marine carbon and oxygen isotope and elemental records indicate icehouse-greenhouse cycles during the Early Jurassic. Paleoceanography 26:PA4219. https://doi.org/10.1029/2011PA002160
Kotake N (1992) Deep-sea echiurans: possible producers of *Zoophycos*. Lethaia 25:311–316. https://doi.org/10.1111/j.1502-3931.1992.tb01400.x
Kotlarczyk J, Uchman A (2012) Integrated ichnology and ichthyology of the Oligocene Menilite Formation, Skole and Subsilesian nappes, Polish Carpathians: a proxy to oxygenation history. Palaeogeogr Palaeoclim Palaeoecol 331–332:104–118. https://doi.org/10.1016/j.palaeo.2012.03.002
Korte C, Hesselbo SP, Ullmann CV, Dietl G, Ruhl M, Schweigert G, Thibault T (2015) Jurassic climate mode governed by ocean gateway. Nat Commun 6:10015. https://doi.org/10.1038/ncomms10015
Krencker FN, Bodin S, Hoffmann R, Suan G, Mattioli E, Kabiri L, Föllmi KB, Immenhauser A (2014) The middle Toarcian cold snap: trigger of mass extinction and carbonate factory demise. Glob Planet Change 117:64–78. https://doi.org/10.1016/j.gloplacha.2014.03.008
Krobicki M, Tyszka J, Uchman A, Bąk M (2006) Stop A2—Flaki Range (Fig. A12B)—Branisko Succesion (Bajocian–Oxfordian). In: Wierzbowski A, Aubrecht R, Golonka J, Gutowski J, Krobicki M, Matyja BA, Pieńkowski G, Uchman A (eds) Jurassic of Poland and Adjacent Slovakian Carpathians, Filed Trip Guidebook of 7th international congress on the Jurassic system, Poland, Kraków, September 6–18, 2006. Polish Geological Institute, Warsaw, pp 29–34
Laskar J, Fienga A, Gastineau M, Manche H (2011) La2010: a new orbital solution for the long term motion of the Earth. Astron Astrophys 532:A89. https://doi.org/10.1051/0004-6361/201116836
Laskar J, Robutel P, Joutel F, Gastineau M, Correia ACM, Levrard B (2004) A longterm numerical solution for the insolation quantities of the Earth. Astron Astrophys 428:261–285. https://doi.org/10.1051/0004-6361:20041335
Laurin J, Meyers SR, Uličný D, Jarvis I, Sageman BB (2015) Axial obliquity control on the greenhouse carbon budget through middle-to high-latitude reservoirs. Paleoceanography 30:133–149. https://doi.org/10.1002/2014PA002736
Li Q, McArthur JM, Thirlwall MF, Turchyn AV, Page K, Bradbury HJ, Weis R, Lowry D (2021) Testing for ocean acidification during the Early Toarcian using δ44/40Ca and δ88/86Sr. Chem Geol 574:120228. https://doi.org/10.1016/j.chemgeo.2021.120228
Littler K, Hesselbo SP, Jenkyns HC (2010) A carbon-isotope perturbation at the Pliensbachian–Toarcian boundary: evidence from the Lias Group, NE England. Geol Mag 147:181–192. https://doi.org/10.1017/S0016756809990458
Locklair RE, Savrda CE (1998) Ichnology of rhythmically bedded Demopolis Chalk (Upper Cretaceous, Alabama): Implications for paleoenvironment, depositional cycle origins, and tracemaker behavior. Palaios 13:423–438. https://doi.org/10.2307/3515472
Lourens LJ (2021) The variation of the Earth's movements (orbital, tilt, and precession) and climate change. In: Lecter TM (ed) Climate change, 3rd edn. Elsevier, Amsterdam, pp 583–606
Löwemark L, Nara M (2013) Morphological variability of the trace fossil *Schaubcylindrichnus coronus* as a response to environmental forcing. Palaeont Electr 16:5A
Löwemark L, Lin I, Sarnthein M (2006) Temporal variations of the trace fossil Zoophycos in a 425 k.y.—long sediment record from the South China Sea: implications for the ethology of the *Zoophycos*-producer. Geol Mag 143:105–114
Macchioni F, Cecca F (2002) Biodiversity and biogeography of middle-late Liassic ammonoids: implications for the early Toarcian mass extinction. Geobios 35(suppl 1):165–175. https://doi.org/10.1016/S0016-6995(02)00057-8
MacEachern JA, Burton JA (2000) Firmground *Zoophycos* in the Lower Cretaceous Viking formation, Alberta: a distal expression of the *Glossifungites* ichnofacies. Palaios 15:387–398. https://doi.org/10.2307/3515511
Maiti S, Tiwari RK (2012) Modeling of rock boundary using Walsh Domain Sequency Filtering: an example from the German Continental Deep Drilling Program (KTB) Borehole Site. In: 9th Biennial international conference and exposition on petroleum geophysics. Society of Petroleum Geophysicists (SPG), Hyderabad 2012, P-019

Mángano MG, Buatois LA (1991) Discontinuity surfaces in the Lower Cretaceus of the High Andes (Mendoza, Argentina): trace fossils and environmental implications. J S Am Earth Sci 4:215–299. https://doi.org/10.1016/0895-9811(91)90032-G

Martinez M, Dera G (2015) Orbital pacing of carbon fluxes by a ~9-My eccentricity cycle during the Mesozoic. Proc Nat Acad Sci 112:12604–12609. https://doi.org/10.1073/pnas.1419946112

Mayer LM (1994) Surface area control of organic carbon accumulation in continental shelf sediments. Geoch Cosmochim Acta 58:1271–1284. https://doi.org/10.1016/0016-7037(94)90381-6

Menini A, Mattioli E, Hesselbo SP, Ruhl M, Suan G (2021) Primary versus carbonate production in the Toarcian, a case study from the Llanbedr borehole (Mochras Farm, Wales). Geol Soc Lond Spec Publ 514:59–81. https://doi.org/10.1144/SP514-2021-19

McArthur JM, Donovan DT, Thirlwall MF, Fouke BW, Mattey D (2000) Strontium isotope profile of the early Toarcian (Jurassic) oceanic anoxic event, the duration of ammonite biozones, and belemnite palaeotemperatures. Earth Planet Sci Lett 179:269–285. https://doi.org/10.1016/S0012-821X(00)00111-4

McArthur JM, Steuber T, Page KN, Landman NH (2016) Sr-isotope stratigraphy: assigning time in the campanian, pliensbachian, toarcian, and valanginian. J Geol 124:541–642. https://doi.org/10.1086/687395

McCave IN (2008) Size sorting during transport and deposition of fine sediments: sortable silt and flow speed. In: Rebesco M, Camerlenghi A (eds) Contourites. Elsevier, Amsterdam, pp 121–142. https://doi.org/10.1016/S0070-4571(08)10008-5

Mikuláš R, Meškis S, Ivanov A, Lukševičs E, Zupinš I, Stinkulis G (2013) A rich ichnofossil assemblage from the Frasnian (Upper Devonian) deposits at Andoma Hill, Onega Lake, Russia. Bull Geosci 88:389–400. https://doi.org/10.3140/bull.geosci.1358

Mulder T (2011) Sedimentary processes and their deposits. In: Huneke H, Mulder T (eds) Deep-sea sediments. Developments in sedimentology, vol 63. Elsevier, Amsterdam, pp 25–148

Müller T, Jurikova H, Gutjahr M, Tomašových A, Schlögl J, Liebetrau V, Duarte LV, Milovsky R, Suan G, Mattioli E, Pittet B, Eisenhauer A (2020) Ocean acidification during the early Toarcian extinction event. Geology 48:1184–1188. https://doi.org/10.1130/G47781.1

Nara M (2006) Reappraisal of *Schaubcylindrichnus*: a probable dwelling/feeding structure of a solitary funnel feeder. Palaeogeogr Palaeoclimat Palaeoecol 240:439–452. https://doi.org/10.1016/j.palaeo.2006.02.015

Naruse H, Nifuku K (2008) Three-dimensional morphology of the ichnofossils *Phycosiphon incertum* and its implication for paleoslope inclination. Palaios 23:270–279. https://doi.org/10.2110/palo.2007.p07-020r

Negi JG, Tiwari RK (1984) Periodicities of palaeomagnetic intensity and palaeoclimatic variations: a Walsh spectral approach. Earth Planet Sci Lett 70:139–147. https://doi.org/10.1016/0012-821X(84)90217-6

Negi JG, Tiwari RK, Rao KN (1993) Comparison of Walsh and Fourier spectroscopy of geomagnetic reversals and nonsinusoidal palaeoclimatic time series. IEEE Trans Geosci Remote Sens 31:127–135. https://doi.org/10.1109/36.210453

Pacześna J (1996) The Vendian and Cambrian ichnocoenoses from the Polish of the East-European Platform. Prace Państw Inst Geol 153:1–77

Pálfy J, Smith PL (2000) Synchrony between Early Jurassic extinction, oceanic anoxic event, and the Karoo-Ferrar flood basalt volcanism. Geology 28:747–750. https://doi.org/10.1130/0091-7613(2000)28%3C747:SBEJEO%3E2.0.CO;2

Pälike H, Norris RD, Herrle JO, Wilson PA, Coxall HK, Lear CH, Shackleton NJ, Tripati AK, Wade BS (2006) The heartbeat of the Oligocene climate system. Science 314:1894–1898. https://doi.org/10.1126/science.1133822

Paulsen M, Thibault N (2023) On the occurrence of rare nannoliths (calcareous nannofossils) in the Early Jurassic and their implications for the end-Triassic mass extinction. Papers in Palaeont e1489. https://doi.org/10.1002/spp2.1489

Pemberton GS, Frey RW (1982) Trace fossil nomenclature and the *Planolites-Palaeophycus* dilemma. J Paleont 56:843–881

Pemberton SG, MacEachern JA, Dashtgard SE, Bann KL, Gingras MK, Zonneveld J-P (2012) Shorefaces. In: Knaust D, Bromley RG (eds) Trace fossils as indicators of sedimentary environments. Developments in sedimentology, vol 64. Elsevier, Amsterdam, pp 563–604. https://doi.org/10.1016/B978-0-444-53813-0.00019-8

Pemberton GS, Spila M, Pulham AJ, Saunders T, MacEachern JA, Robbins D, Sinclair IK (2001) Ichnology and sedimentology of shallow to marginal marine systems: Ben Nevis & Avalon Reservoirs, Jeanne D'Arc Basin. Geological Association of Canada, Short Course Notes 15

Pervesler P, Uchman A (2004) Ichnofossils from the type area of the Grund Formation (Miocene, Lower Badenian) in northern Lower Austria (Molasse Basin). Geol Carpath 55:103–110

Pervesler P, Uchman A, Hohenegger J (2008) New methods for ichnofabric analysis and correlation with orbital cycles exemplified by the Baden-Sooss section (Middle Miocene, Vienna Basin, Lower Austria). Geol Carpath 59:395–409

Pieńkowski G (1985) Early Liassic trace fossils assemblages from the Holy Cross Mountains, Poland: their distribution in continental and marginal marine environments. In: Curran AH (ed) Biogenic structures: their use in interpreting depositional environments. Soc Econ Paleont Miner Spec Publ 35:37–51

Pieńkowski G (2004) The epicontinental Lower Jurassic of Poland. Pol Geol Inst Spec Pap 12:1–154

Pieńkowski G, Hodbod M, Ullmann CV (2016) Fungal decomposition of terrestrial organic matter accelerated Early Jurassic climate warming. Sci Rep 6:31930. https://doi.org/10.1038/srep31930

Pieńkowski G, Uchman A, Ninard K, Hesselbo SP (2021) Ichnology, sedimentology, and orbital cycles in the hemipelagic Early Jurassic Laurasian Seaway (Pliensbachian, Cardigan Bay Basin, UK). Glob Planet Change 207:103648. https://doi.org/10.1016/j.gloplacha.2021.103648

Pollard JE (1988) Trace fossils in coal-bearing sequence. J Geol Soc Lond 145:339–350. https://doi.org/10.1144/gsjgs.145.2.033

Powell JH (2010) Jurassic sedimentation in the Cleveland Basin: a review. Proc Yorkshire Geol Soc 58:21–72. https://doi.org/10.1144/pygs.58.1.278

Rebesco M, Wåhlin A, Laberg JS, Schauer A, Beszczynska-Möller A, Lucchi RG, Noormets R, Accettella D, Zarayskaya Y, Diviacco P (2013) Quaternary contourite drifts of the Western Spitsbergen margin. Deep-Sea Res Part I Oceanogr Res Pap 79:156–168. https://doi.org/10.1016/j.dsr.2013.05.013

Rebesco M, Hernández-Molina FJ, Van Rooij D, Wåhlin A (2014) Contourites and associated sediments controlled by deep-water circulation processes: state of the art and future considerations. Mar Geol 352:111–154. https://doi.org/10.1016/j.margeo.2014.03.011

Reggiani L, Mattioli Pittet E, Duarte LV, Veiga de Oliveirae LC, Comas-Rengifo MJ (2010) Pliensbachian (Early Jurassic) calcareous nannofossils from the Peniche section (Lusitanian Basin Portugal): a clue for palaeoenvironmental reconstructions. Mar Micropaleontol 75:1–16. https://doi.org/10.1016/j.marmicro.2010.02.002

Remirez MN, Algeo TJ (2020) Paleosalinity determination in ancient epicontinental seas: a case study of the T-OAE in the Cleveland Basin (UK). Earth Sci Rev 201:103072. https://doi.org/10.1016/j.earscirev.2019.103072

Reolid M, Copestake P, Johnson B (2019) Foraminiferal assemblages, extinctions and appearances associated with the Early Toarcian Oceanic Anoxic Event in the Llanbedr (Mochras Farm) Borehole, Cardigan Bay Basin, United Kingdom. Palaeogeogr Palaeoclimatol Palaeoecol 532:109277. https://doi.org/10.1016/j.palaeo.2019.109277

Rocha RB, Mattioli E, Duarte LV, Pittet B, Elmi S, Mouterde R, Cabral MC, Comas-Rengifo MJ, Gómez JJ, Goy A, Hesselbo SP, Jenkyns HC, Littler K, Mailliot S, de Oliveira CV, Osete ML, Perilli N, Pinto S, Ruget C, Suan G (2016) Base of the Toarcian Stage of the Lower Jurassic defined by the Global Boundary Stratotype Section and Point (GSSP) at the Peniche Section (Portugal). Episodes 39:460–481. https://doi.org/10.18814/epiiugs/2016/v39i3/99741

Rodriguez-Tovar FJ, Nagy J, Reolid M (2014) Palaeoenvironment of Eocene prodelta in Spitsbergen recorded by the trace fossil *Phycosiphon incertum*. Polar Res 33:23786. https://doi.org/10.3402/polar.v33.23786

Rodríguez-Tovar FJ, Mena A, Hernández-Molina FJ, Dorador J (2016) Incidence of bioturbation on grain size redistribution: preventing misinterpretations in sedimentary analysis. Geo-Temas 16:291–294

Rodríguez-Tovar FJ, Dorador J, Mena A, Hernández-Molina FJ (2017) Improving ichnofabric analysis in cores: computed tomography images and high resolution digital treatment. In: 14th International ichnofabric workshop, Taipei, Taiwan, Abstract Volume. TPE, Taipei, p 47

Rodríguez-Tovar FJ, Hernández-Molina FJ (2018) Ichnological analysis of contourites: past, present and future. Earth Sci Rev 182:28–41. https://doi.org/10.1016/j.earscirev.2018.05.008

Rodríguez-Tovar FJ, Hernández-Molina FJ, Hüneke H, Chiarella D, Llave E, Mena A, Miguez-Salas O, Dorador J, de Castro S, Stow DAV (2019a) Key evidence for distal turbiditic- and bottom-current interactions from tubular turbidite infills. Palaeogeog Palaeoclim Palaeoecol 533:109233. https://doi.org/10.1016/j.palaeo.2019.109233

Rodríguez-Tovar FJ, Hernández-Molina FJ, Hüneke H, Llave E, Stow D (2019b) Contourite facies model: improving contourite characterization based on the ichnological analysis. Sediment Geol 384:60–69. https://doi.org/10.1016/j.sedgeo.2019.03.010

Rodríguez-Tovar FJ, Pardo-Igúzquiza E, Reolid M (2020) Cyclic environmental changes during the Early Toarcian at the Mochras Farm Borehole (Wales): a variable response of the foraminiferal community. Lethaia 54:113–126. https://doi.org/10.1111/let.12392

Rodríguez-Tovar FJ, Miguez-Salas O, Dorador J (2022) Deepwater ichnology: new observations on contourites. In: Rotzien JR, Yeilding CA, Sears RA, Hernández-Molina FJ, Catuneanu O (eds) Deepwater sedimentary systems. Elsevier, Amsterdam, pp 253–554

Ruebsam W, Al-Husseini M (2021) Orbitally synchronized late Pliensbachian–early Toarcian glacio-eustatic and carbon-isotope cycles. Palaeogeogr Palaeoclim Palaeoecol 577:110562. https://doi.org/10.1016/j.palaeo.2021.110562

Ruebsam W, Reolid M, Sabatino N, Masetti D, Schwark L (2020) Molecular paleothermometry of the early Toarcian climate perturbation. Glob Planet Change 195:103351. https://doi.org/10.1016/j.gloplacha.2020.103351

Ruhl M, Hesselbo SP, Hinnov L, Jenkyns HC, Xu W, Storm MS, Riding JB, Minisini D, Ullmann CV, Leng MJ (2016) Astronomical constraints on the duration of the Early Jurassic Pliensbachian Stage and global climatic fluctuations. Earth Planet Sci Lett 455:149–165. https://doi.org/10.1016/j.epsl.2016.08.038

Ruhl M, Hesselbo SP, Jenkyns HC, Xu W, Silva RL, Matthews KJ, Mather TA, Mac Niocaill C, Riding JB (2022) Reduced plate movement controlled onset and timing of Early Jurassic (Toarcian) Karoo-Ferrar large igneous province volcanism and global environmental change. Sci Adv 8:eabo0866. https://doi.org/10.1126/sciadv.abo0866

Ruvalcaba Baroni I, Pohl A, van Helmond NAGM, Papadomanolaki NM, Coe AL, Cohen AS, van de Schootbrugge B, Donnadieu Y, Slomp CP (2018) Ocean circulation in the Toarcian (Early Jurassic): a key control on deoxygenation and carbon burial on the European shelf. Paleoceanogr Paleoclimat 33:994–1012. https://doi.org/10.1029/2018PA003394

Savarese M, Dodd JR, Lane NG (1997) Taphonomic and sedimentologic implications of crinoid intraskeletal porosity. Lethaia 29:141–156. https://doi.org/10.1111/j.1502-3931.1996.tb01870.x

Savrda CE, Krawinkel H, McCarthy FMG, McHugh CMG, Olson HC, Mountain G (2001) Ichnofabrics of a Pleistocene slope succession, New Jersey in relation to climate and sea-level dynamics. Palaeogeogr Palaeoclimat Palaeoecol 171:41–61. https://doi.org/10.1016/S0031-0182(01)00266-8

Schlirf M (2000) Upper Jurassic trace fossils from the Boulonnais (northern France). Geol Palaeont 34:145–213

Schlirf M, Uchman A (2005) Revision of the ichnogenus *Sabellarifex* Richter, 1921 and its relationship to *Skolithos* Haldeman, 1840 and *Polykladichnus* Fürsich, 1981. J Syst Palaeont 3:115–131. https://doi.org/10.1017/S1477201905001550

Schlirf M, Uchman A, Kümmel M (2001) Upper Triassic (Keuper) non-marine trace fossils from the Haßberge area (Franconia, south-eastern Germany). Paläont Zeitschr 75:71–96. https://doi.org/10.1007/BF03022599

Sell B, Ovtcharova M, Guex J, Bartolini A, Jourdan F, Spangenberg JE, Vicente JC, Schaltegger U (2014) Evaluating the temporal link between the Karoo LIP and climatic–biologic events of the Toarcian Stage with high-precision U–Pb geochronology. Earth Planet Sci Lett 408:48–56. https://doi.org/10.1016/j.epsl.2014.10.008

Sellwood BW (1972) Regional environmental changes across a Lower Jurassic stage-boundary in Britain. Palaeontology 15:125–157

Shanmugam G (2000) 50 years of the turbidite paradigm (1950s–1990s), deep-water processes and facies models: a critical perspective. Mar Petrol Geol 17:285–342. https://doi.org/10.1016/S0264-8172(99)00011-2

Shanmugam G (2008) Deep-water bottom currents and their deposits. In: Rebesco M, Camerlenghi A (eds) Contourites. Developments in sedimentology, vol 60. Elsevier, Amsterdam, pp 59–83. https://doi.org/10.1016/S0070-4571(08)10005-X

Shanmugam G (2017) Contourites: physical oceanography, process sedimentology, and petroleum geology. Petrol Explor Dev 44:183–216. https://doi.org/10.1016/S1876-3804(17)30023-X

Stachacz M (2016) Ichnology of the Cambrian Ociesęki Sandstone Formation (Holy Cross Mountains, Poland). Ann Soc Geol Polon 86:291–328. https://doi.org/10.14241/asgp.2016.007

Stanistreet IG, Le Blanc Smith GK, Cadle AB (1980) Trace fossils as sedimentological and palaeoenvironmental indices in the Ecca Group (Lower Permian) of the Transvaal. Trans Geol Soc S Afr 83:333–344

Storm MS, Hesselbo SP, Jenkyns HC, Ruhl M, Ullmann CV, Xu W, Leng MJ, Riding JB, Gorbanenko O (2020) Orbital pacing and secular evolution of the Early Jurassic carbon cycle. Proc Nat Acad Sci USA 117:3974–3982. https://doi.org/10.1073/pnas.1912094117

Stow DAV, Holbrook JA (1984) North Atlantic contourites: an overview. In: Stow DAV, Piper DJW (eds) Fine-grained sediments, deep-water processes and facies. Geol Soc London Spec Publ 15:245–256. https://doi.org/10.1144/GSL.SP.1984.015.01.16

Stow DAV, Faugeres JC (2008) Contourite facies and the facies model. In: Rebesco M, Camerlenghi A (eds) Contourites. Developments in sedimentology, vol 60. Elsevier, Amsterdam, pp 223–256. https://doi.org/10.1016/S0070-4571(08)10013-9

Stow DAV, Faugères J-C, Howe JA, Pudsey CJ, Viana AR (2002) Bottom currents, contourites and deep-sea sediment drifts: current state-of-the-art. In: Stow DAV, Pudsey CJ, Howe JA, Faugères J-C, Viana AR (eds) Deep-Water Contourite Systems: Modern Drifts and Ancient Series:Seismic and Sedimentary Characteristics. Geol Soc London Mem 22:7–20. https://doi.org/10.1144/GSL.MEM.2002.022.01.02

Suan G, Pittet B, Bour I, Mattioli E, Duarte LV, Mailliot S (2008) Duration of the Early Toarcian carbon isotope excursion deduced from spectral analysis: consequence for its possible causes. Earth Planet Sci Lett 267:666–679. https://doi.org/10.1016/j.epsl.2007.12.017

Suan G, Mattioli E, Pittet B, Lécuyer C, Suchéras-Marx B, Duarte LV, Philippe M, Reggiani L, Martineau F (2010) Secular environmental precursors to Early Toarcian (Jurassic) extreme climate changes. Earth Planet Sci Lett 290:448–458. https://doi.org/10.1016/j.epsl.2009.12.047

Suess E (1980) Particulate organic carbon flux in the oceans: surface productivity and oxygen utilization. Nature 288:260–263. https://doi.org/10.1038/288260a0

Surlyk F, Lykke-Andersen H (2007) Contourite drifts, moats and channels in the Late Cretaceous chalk of the Danish Basin. Sedimentology 54:405–422. https://doi.org/10.1111/j.1365-3091.2006.00842.x

Taylor A, Goldring R, Gowland S (2003) Analysis and application of ichnofabrics. Earth Sci Rev 60:227–259. https://doi.org/10.1016/S0012-8252(02)00105-8

Thistle D, Yingst JY, Fauchald K (1985) A deep-sea benthic community exposed to strong near-bottom currents on the Scotian Rise (western Atlantic). Mar Geol 66:91–112. https://doi.org/10.1016/0025-3227(85)90024-6

Thistle D, Ertman SC, Fauchald K (1991) The fauna of the HEBBLE site: patterns in standing stock and sediment-dynamic effects. Mar Geol 99:413–422. https://doi.org/10.1016/0025-3227(91)90053-7

Tiwari RK (1987) A Walsh spectral comparison of oxygen ($\delta^{18}O$) and carbon isotope ($\delta^{13}C$) variations of the Pleistocene bore hole (Eureka 67–135) from the Gulf of Mexico and their orbital significance. Mar Geol 78:167–174. https://doi.org/10.1016/0025-3227(87)90076-4

Tucholke BE, Hollister CD, Biscaye PE, Gardner WD (1985) Abyssal current character determined from sediment bedforms on the Nova Scotian continental Rise. Mar Geol 66:43–57. https://doi.org/10.1016/0025-3227(85)90022-2

Uchman A (1992) Ichnogenus *Rhizocorallium* in the Paleogene flysch (Outer Western Carpathians, Poland). Geol Carpath 43:57–60

Uchman A (1995) Taxonomy and palaeoecology of flysch trace fossils: The Marnoso-arenacea Formation and associated facies (Miocene, Northern Apennines, Italy). Beringeria 15:3–115

Uchman A (1998) Taxonomy and ethology of flysch trace fossils: a revision of the Marian Książkiewicz collection and studies of complementary material. Ann Soc Geol Polon 68:105–218

Uchman A (1999) Ichnology of the Rhenodanubian Flysch (Lower Cretaceous–Eocene) in Austria and Germany. Beringeria 25:65–171

Uchman A, Tchoumatchenco P (2003) A mixed assemblage of deep-sea and shelf trace fossils from the Lower Cretaceous (Valanginian) Kamchia

Formation in the Troyan region, central Fore-Balkan, Bulgaria. Ann Soc Geol Polon 73:27–34
Uchman A, Wetzel A (2011) Deep-sea ichnology: the relationships between depositional environment and endobenthic organisms. In: Hüneke H, Mulder T (eds) Deep-sea sediments. Developments in sedimentology, vol 63. Elsevier, Amsterdam, pp 517–556. https://doi.org/10.1016/B978-0-444-53000-4.00008-1
Ullmann CV, Boyle B, Duarte LV, Hesselbo SP, Kasemann S, Klein T, Lenton T, Piazza V, Aberhan M (2020) Warm afterglow from the Toarcian Oceanic Anoxic Event drives the success of deep-adapted brachiopods. Sci Rep 10:6549
Ullmann CV, Szűcs D, Jiang M, Hudson AJL, Hesselbo SP (2021) Geochemistry of macrofossil, bulk rock, and secondary calcite in the Early Jurassic strata of the Llanbedr (Mochras Farm) drill core, Cardigan Bay Basin, Wales, UK. J Geol Soc Lond 179:jgs2021-018. https://doi.org/10.1144/jgs2021-018
Vahlenkamp M, Niezgodzki I, De Vleeschouwer D, Bickert T, Harper D, Kirtland Turner S, Lohmann G, Sexton P, Zachos J, Pälike H (2018) Astronomically paced changes in deep-water circulation in the western North Atlantic during the middle Eocene. Earth Planet Sci Lett 484:329–340. https://doi.org/10.1016/j.epsl.2017.12.016
Van Echelpoel E (1994) Identification of regular sedimentary cycles using Walsh spectral analysis with results from the Boom Clay Formation, Belgium. In: de Boer PL, Smith D (eds) Orbital forcing and cyclic sequences. Spec Publ Internat Assoc Sedimentol 19:63–76
Van Rooij D, Iglesia J, Hernández-Molina FJ, Ercilla G, Gomez-Ballesteros M, Casas D, Llave E, De Hauwere A, Garcia-Gil S, Acosta J, Henriet J-P (2010) The Le Danois contourite depositional system: interactions between the Mediterranean Outflow Water and the upper Cantabrian slope (North Iberian margin). Mar Geol 274:1–20. https://doi.org/10.1016/j.margeo.2010.03.001
Van de Schootbrugge B, Houben AJP, Ercan FEZ, Verreussel R, Kerstholt S, Janssen NMM, Nikitenko B, Suan G (2019) Enhanced Arctic-Tethys connectivity ended the Toarcian Oceanic Anoxic Event in NW Europe. Geol Mag 157:1593–1611. https://doi.org/10.1017/S0016756819001262
Voigt E, Häntzschel W (1956) Die grauen Bänder in der Schreibkreide Nordwest-Deutschlands und ihre Deutung als Lebensspuren. Mitt Geol Staatsinst Hamburg 25:104–122
Vörös A (2002) Victims of the Early Toarcian anoxic event: the radiation and extinction of Jurassic Koninckinidae (Brachiopoda). Lethaia 35:345–357. https://doi.org/10.1111/j.1502-3931.2002.tb00093.x
Waltham D (2015) Milankovitch period uncertainties and their impact on cyclostratigraphy. J Sediment Res 85:990–998. https://doi.org/10.2110/jsr.2015.66
Wang Y, Wang X, Hu B, Uchman A (2019) Burrows of the polychaete *Perinereis aibuhiutensis* on a tidal flat of Yellow River Delta in China: implications for the ichnofossils *Polykladichnus* and *Archaeonassa*. Palaios 34:271–279. https://doi.org/10.2110/palo.2018.105
Weedon G (1989) The detection and illustration of regular sedimentary cycles using Walsh power spectra and filtering, with examples from the Lias of Switzerland. J Geol Soc 146:133–144. https://doi.org/10.1144/gsjgs.146.1.0133
Weedon G (2003) Time-series analysis and cyclostratigraphy: examining stratigraphic records of environmental cycles. Cambridge University Press, Cambridge
Westergård AH (1931) *Diplocraterion*, *Monocraterion* and *Scolithus*. Sver Geol Undersöknig ÅRsbok Ser C 25:3–25
Wetzel A (1981) Ökologische und stratigraphische Bedeutung biogener Gefüge in quartären Sedimenten am NW-afrikanischen Kontinentalrand. "Meteor" Forsch-Ergebnisse. Reihe C 34:1–47
Wetzel A (1983) Biogenic structures in modern slope to deep-sea sediments in the Sulu Sea Basin (Philippines). Palaeogeogr Palaeoclim Palaeoecol 42:285–304
Wetzel A (1991) Ecologic interpretation of deep-sea trace fossil communities. Palaeogeogr Palaeoclim Palaeoecol 85:47–69. https://doi.org/10.1016/0031-0182(83)90027-5
Wetzel A (2007) Ichnofabrics in Eocene to Maestrichtian sediments from Deep Sea Drilling Project Site 605, off the New Jersey coast. Deep Sea Drill Proj Rep Publ 93:825–835. https://doi.org/10.2973/dsdp.proc.93.129.1987
Wetzel A (2008) Recent bioturbation in the deep South China Sea: a uniformitarian ichnologic approach. Palaios 23:601–615. https://doi.org/10.2110/palo.2007.p07-096r
Wetzel A (2010) Deep-sea ichnology: observations in modern sediments to interpret fossil counterparts. Acta Geol Polon 60:125–138
Wetzel A, Blechschmidt I, Uchman A, Matter A (2007) A highly diverse ichnofauna in late Triassic deep-sea fan deposits of Oman. Palaios 22:567–576. https://doi.org/10.2110/palo.2006.p06-098r
Wetzel A, Bromley RG (1994) *Phycosiphon incertum* revisited: *Anconichnus horizontalis* is its junior subjective synonym. J Paleont 68:1396–1402. https://doi.org/10.1016/S0031-0182(00)00254-6
Wetzel A, Uchman A (2001) Sequential colonization of muddy turbidites: examples from Eocene Beloveža Formation, Carpathians, Poland. Palaeogeogr Palaeoclim Palaeoecol 168:171–186. https://doi.org/10.1016/S0031-0182(00)00254-6
Wetzel A, Uchman A (2012) Hemipelagic and pelagic basin plains. In: Bromley RG, Knaust D (eds) Trace fossils as indicators of sedimentary environments. Developments in Sedimentology, vol 64. Elsevier, Amsterdam, pp 673–701. https://doi.org/10.1016/B978-0-444-53813-0.00022-8
Wetzel A, Werner F (1981) Morphology and ecological significance of *Zoophycos* in deep-sea sediments off NW Africa. Palaeogeogr Palaeoclim Palaeoecol 32:185–212. https://doi.org/10.1016/0031-0182(80)90040-1
Wetzel A, Werner F, Stow DAV (2008) Bioturbation and biogenic sedimentary structures in contourites. In: Rebesco M, Camerlenghi A (eds) Contourites. Developments in sedimentology, vol 60. Elsevier, Amsterdam, pp 183–202. https://doi.org/10.1016/S0070-4571(08)10011-5
Winguth AME, Maier-Reimer E (2005) Causes of marine productivity and oxygen changes associated with the Permian-Triassic boundary: a reevaluation with ocean general circulation models. Mar Geol 217:283–304. https://doi.org/10.1016/j.margeo.2005.02.011
Winguth AME, Heinze C, Kutzbach JE, Maier-Reimer E, Mikolajewicz U, Rowley D, Rees A, Ziegler AM (2002) Simulated warm polar currents during the middle Permian. Paleoceanography 17:1057. https://doi.org/10.1029/2001PA000646
Woodland AW (ed) (1971) The Llanbedr (Mochras Farm) Borehole. Report No. 71/18, Institute of Geological Sciences
Wu H, Hinnov LA, Zhang S, Jiang G, Yang T, Li H, Xi D, Ma X, Wang C (2022) Continental geological evidence for Solar System chaotic behavior in the Late Cretaceous. Geol Soc Am Bull 135:212–226. https://doi.org/10.1130/B36340.1
Xu W, Ruhl M, Jenkyns HC, Leng MJ, Huggett JM, Minisini D, Ullmann CV, Riding JB, Weijers JWH, Storm MS, Percival LME, Tosca NJ, Idiz EF, Tegelaar EW, Hesselbo SP (2018a) Evolution of the Toarcian (Early Jurassic) carbon-cycle and global climatic controls on local sedimentary processes (Cardigan Bay Basin, UK). Earth Planet Sci Lett 484:396–411. https://doi.org/10.1016/j.epsl.2017.12.037
Xu W, MacNiocaill C, Ruhl M, Jenkyns HC, Riding JB, Hesselbo SP (2018b) Magnetostratigraphy of the Toarcian Stage (Lower Jurassic) of the Llanbedr (Mochras Farm) borehole, Wales: basis for a global standard and implications for volcanic forcing of palaeoenvironmental change. J Geol Soc 175:594604. https://doi.org/10.1144/jgs2017-120
Zhang L-J, Fan R-Y, Gong Y-M (2015) *Zoophycos* macroevolution since 541 Ma. Nature Sci Rep 5(14954):1–10. https://doi.org/10.1038/srep14954

Publisher's Note